Swing, release, and escape mechanisms contribute to the generation of phase-locked cluster patterns in a globally coupled FitzHugh-Nagumo model

.

NJIT CAMS Technical Report
1112-9

Horacio G. Rotstein* and Hui Wu
Department of Mathematical Sciences
New Jersey Institute of Technology
Newark, NJ 07102, USA

September 24, 2012

Abstract

We investigate the mechanism of generation of phase-locked cluster patterns in a globally coupled FitzhHugh-Nagumo model where the fast variable (activator) receives global feedback from the slow variable (inhibitor). We identify three qualitatively different mechanisms (swing-and-release, hold-and-release, and escape-and-release) that contribute to the generation of these patterns. We describe these mechanisms and use this framework to explain under what circumstances two initially out-of-phase oscillatory clusters reach steady phase-locked and in-phase synchronized solutions, and how the phase difference between these steady state cluster patterns depends on the clusters relative size, the global coupling intensity, and other model parameters.

1 Introduction

Oscillatory patterns are frequently observed in nonlinear, far from equilibrium chemical, biochemical and biological systems [1, 2, 3, 4, 5, 6]. Oscillations are observed in some key variables such as

*Also, Center for Applied Mathematics and Statistics, New Jersey Institute of Technology. E-mail: horacio@njit.edu

concentrations in chemical and biochemical reactions [7, 8, 9] and voltage and gating variables in neural systems [5]. These variables have been classified into activators and inhibitors. The former stimulate both their own production via autocatalytic effects (positive feedback) and the production of the inhibitor. The latter repress the production of the activator (negative feedback). Inhibitors are also referred to as recovery variables.

Globally coupled oscillatory systems have been studied both experimentally and theoretically in a variety of systems including chemical reactions [10, 11, 12, 13, 14, 15], metabolic oscillators [16, 17], electrochemical oscillators [18, 19, 20, 21, 22, 23, 24, 25, 26, 27, 28], catalytic reactions [29], neuronal networks [5, 30, 31, 32, 33, 34, 35], salt-water oscillators [36], laser arrays [37], and cardiac oscillators [38, 39]. Theoretical studies have been performed using activator-inhibitor type models that explicitely describe the dynamics of the participating physical (chemical, biological, etc) variables. Oscillatory patterns in globally coupled models have also been studied using the so called phase oscillators [40, 41, 42, 43, 44, 45, 46]. In these models, each oscillator is described solely by its phase and the effects of the interaction of oscillators on their amplitude is neglected by assuming weak coupling.

This paper is motivated by the oscillatory cluster patterns observed in the Belousov-Zhabotinsky (BZ) reaction with photochemical global feedback (global coupling) [10, 11]. The BZ reaction is the prototypical example of nonlinear chemical oscillators [47, 48, 49, 50]. It consists on the oxidation of malonic acid by bromate ions in an acid medium and in the presence of a catalyst with two ionization states. Oscillations are observed in the concentration of these ions and reflected in changes in the color of the solution. Photochemical global feedback is imposed through illumination in the photosensitive BZ reaction using the photosensitive catalyst Rubipy . The average concentration of the catalyst (an inhibitor) taken over the working area of the gel is employed to control the intensity of actinic light [10, 11].

Oscillatory clusters are sets of oscillators, or domains, in which nearly all elements in a given domain oscillate with the same amplitude and phase (i.e., they are synchronized in-phase) [30, 41, 13, 14]. Three important cluster patterns observed in the BZ reaction with global inhibitory feedback are two-phase, three-phase and localized clusters [10]. The former two consist of two or three clusters oscillating out-of-phase. The latter consists of a two-phase clusters in one region of the reactor while the reminder shows no oscillations or oscillations with a very small amplitude.

Simulations using the Oregonator and a modified version of the Oregonator [51] both with globally inhibitory feedback reproduce the experimental results [10, 12]. The mechanism of generation of localized clusters has been studied in [14] using this model and in [13] using a modified version of the FitzHugh-Nagumo (FHN) model. The mechanisms underlying the generation of phase-locked, two-cluster patterns are not well understood.

In this paper, we aim to understand fundamental aspects of the mechanism of generation of these patterns in a FHN model with a global feedback term qualitatively similar to the one used in [11, 12, 13, 14] where the activator equation receives global feedback from the inhibitor variable. Models of FHN type [52, 53, 54] are simplified caricature models of the Oregonator and other types of models (e.g., the Morris-Lecar model [55] for neurons) that conserve their main relevant features such as the cubic shapes of the nullcline for the activator and the bifurcation structure. The principles that emerge from our study can be applied to the investigation of other, qualitatively similar, activator-

inhibitor systems and patterns with a larger number of clusters.

We use a self-consistent argument by assuming the existence of two clusters with the same or different sizes, initially oscillating out-of-phase. We investigate under what circumstances the two clusters reach out-of-phase (phase-locked) and in-phase steady solutions, and how the phase difference of these steady cluster patterns (defined precisely below) depends on the clusters relative size and other model parameters.

We have identified three qualitatively different basic mechanisms: *swing-and-release*, *hold-and-release*, and *hold-and-escape*. The *swing-and-release* mechanism is related to the canard phenomenon. The *hold-and-release* and *hold-and-escape* mechanisms are related to the release and escape mechanisms in synaptically connected neural models [56, 57, 58]. We use simulations and dynamical systems tools to explain how, and under what circumstances, these basic mechanisms contribute to the generation of phase-locked patterns in the globally coupled FHN model we investigate. A more rigorous mathematical treatment will be done elsewhere.

In this paper, we disregard spatial structure; i.e., oscillators in each cluster do not need to be spatially grouped. We focus on the mechanism by which clusters are generated and not on the mechanism by which oscillators within a cluster group into spatially extended domains.

The overview of the paper is as follows. In Section 2 we first introduce the globally coupled FHN model we study in this paper. Then, we describe the cluster simplification method that allows us to reduce a large system of globally coupled oscillators into a system of two globally coupled oscillators representing two clusters. Differences in the cluster sizes translate into weights in the global coupling terms. Finally, we discuss the canard phenomenon that plays an important role in the mechanism of generation of phase-locked clusters. In Section 3 we discuss the basic mechanisms mentioned above (swing-and-release, hold-and-release, and escape-and-release) that contribute to the generation of phase-locked patterns. In Sections 4 and 5 we explain how in-phase and phase-locked patterns emerge in globally coupled system consisting of two clusters with the same and different sizes respectively. We discuss our results in Section 6.

2 Models, strategy and background

2.1 FitzHugh-Nagumo model

The general form of the FitzHugh-Nagumo (FHN) model we use here is

$$\begin{cases} v' = f(v) - w, \\ w' = \epsilon\,[\,\alpha\, v - \lambda - w\,] \end{cases} \tag{1}$$

where $\alpha > 0$, $0 < \epsilon \ll 1$ and λ are constants, and $f(v) - 2\ v^3 + 3\ v^2$ is a cubic function having a minimum at $(0,0)$ and a maximum at $(1,1)$. The magnitude of the parameter ϵ, representing the time scale separation between the two variables v and w, indicates that system (1) is a fast-slow system. The v- and w-nullclines are given by $w = N_v(v) = f(v)$ and $w = N_w(v) = \alpha\, v - \lambda$. The parameters α and λ control the slope of the w-nullcline and its displacement with respect to the

v-nullcline respectively. The phase-plane and traces (graphs of v and w vs. t) for a representative set of parameters are shown in Fig. 1. The relaxation oscillations for are qualitatively similar to these displayed by the Oregonator model [14].

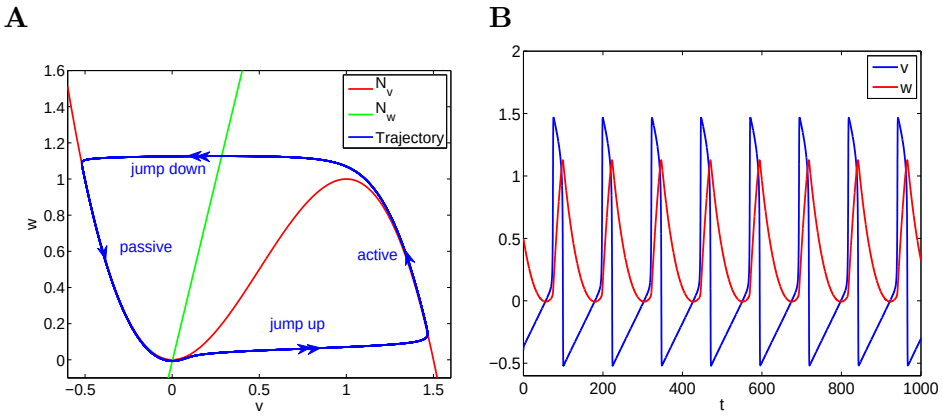

Figure 1: **Fast-slow oscillations (relaxation-type) in the FitzHugh-Nagumo model for a representative set of parameters. A.** Phase-plane. During the slow phases the limit cycle trajectory (blue) is very close (almost superimposed) to the cubic v-nullcline (red). **B** Traces (graphs of v and w vs. t). We used the following parameter values $\alpha = 2$, $\lambda = 0.01$ and $\epsilon = 0.01$.

2.2 Globally coupled FitzHugh-Nagumo model

Following the experimental setup for the globally coupled photosensitive BZ reaction, Oregonator models have been extended to include a term representing a global feedback from the inhibitor variable (w) to the activator variable (v) [10, 12, 14]. The analogous equations for a discrete system of N oscillators of FHN type read [13]

$$\begin{cases} v_k' = f(v_k) - w_k + \Gamma_{N,w}, & k = 1, \ldots, N, \\ w_k' = \epsilon\,[\,\alpha\, v_k - \lambda - w_k\,], \end{cases} \tag{2}$$

where the global coupling term $\Gamma_{N,w}$ is given by

$$\Gamma_{N,w} = -\gamma\ (\ < w > - w_{tgt}\ ) \qquad \text{with} \qquad < w >= \frac{1}{N}\sum_{k=1}^{N} w_k. \tag{3}$$

In (3), $\gamma \geq 0$ (global feedback parameter) and w_{tgt} is a constant. The original choice for w_{tgt} in [10] was the w-coordinate ($\bar{w}$) of the fixed-point (intersection between the nullclines) (see also [13, 14]). For this choice of w_{tgt}, the intersection point between the v_k- and w_k-nullclines is independent of γ. In [13] we have used a similar global feedback term to investigate the mechanism of generation of localized solutions in a modified version of the globally coupled FHN model. Other studies have

considered global feedback from the activator variable onto itself, rather than from the inhibitor onto the activator variables, either directly [35, 59, 60, 61, 62]

$$\Gamma_{N,v} = -\gamma \, (< v > - v_{tgt} \,) \qquad \text{with} \qquad < v >= \frac{1}{N} \sum_{k=1}^{N} v_k \tag{4}$$

or through a synaptic function [63, 32, 64, 31, 65]. Note that there is a difference between global inhibition and the global effect of an inhibitor variable. Inhibition refers to the "negative" effect of either an activator or inhibitor variable. When $\Gamma_{N,w} < 0$ uniformly, system (3) is globally inhibited through the inhibitory variable. Here, we focus on global feedback of the form (3). Note that the value of w_{tgt} can be used to control the sign of the global feedback term.

2.3 Cluster reduction

Our operational definition of a cluster is a set of identical oscillators synchronized in phase. A *cluster reduction* consists in assuming that the N globally coupled oscillators are divided into two groups (or clusters). The dynamics of each cluster can be described using the same equations as for the corresponding oscillators. For a two-cluster system, $< w >= \sigma_1 w_1 + \sigma_2 w_2$ with σ_1 and σ_2 representing the fraction of oscillators belonging to each cluster ($\sigma_1 + \sigma_2 = 1$). The FHN equations for a two-cluster system with global coupling (2) through the inhibitor (cluster) variables w_1 and w_2 read

$$\begin{cases} v_k' = f(v_k) - (1 + \sigma_k \, \gamma) \, w_k + \gamma \, w_{tgt} - \gamma \; \sigma_j \, w_j, & k, j = 1, 2, \quad j \neq k \\ w_k' = \epsilon \; [\, \alpha \, v_k - \lambda - w_k \,]. \end{cases} \tag{5}$$

The zero-level surfaces ("higher-dimensional nullclines") are given by

$$w_k = N_{v,k}(v_k, w_j) = \frac{f(v_k) + \gamma \, w_{tgt}}{1 + \sigma_k \gamma} - \frac{\gamma \, \sigma_j w_j}{1 + \sigma_k \gamma} \qquad k, j = 1, 2, \quad j \neq k \tag{6}$$

and $w_k = N_{w,k}(v_k) = \alpha \, v_k - \lambda$, $k = 1, 2$. Eq. (6) describes a two-dimensional surface having the shape of the first term in the right hand side in eq. (6), $N_{v,k}(v_k, 0)$. For $\gamma > 0$, the nullsurface (6) can be thought of as the v-nullcline $f(v)$ of the k^{th} oscillator for $\gamma = 0$, deformed (raised by an amount $\gamma \, w_{tgt}$ and flattened by the effect of the denominator), and forced by the second oscillator via the function $w_j(t)$ ($j \neq k$). We refer to $N_{v,k}(v_k, 0)$ as the v_k-nullcline. Oscillations in $w_j(t)$ "raise" and "lower" this v_k-nullcline. As a consequence, the intersection point with the (fixed) w_k-nullcline "moves" describing a curve parametrized by t. Points in this curve are not fixed-points of the four dimensional system. However, they play a significant role in organizing the dynamics of the coupled system. We refer to them as "effective fixed-points" (or just fixed-points). Since the curve of effective fixed-points is parametrized by t, as t progresses, the relative position between them and the minimum of the v-nullcline also changes. As we show below, this will have a significant effect in determining the evolution of trajectories in phase-space.

2.4 The canard phenomenon and sensitivity to transient perturbations

In two-dimensional relaxation oscillators such as systems (1) with $\epsilon \ll 1$, the canard phenomenon (or canard explosion) refers to the abrupt increase in the amplitude of the limit cycle created in a Hopf bifurcation as a control parameter crosses a very small critical range which is exponentially small in ϵ [66, 67, 68, 69, 70, 71, 72]. Depending on whether the Hopf bifurcation is supercritical or subcritical, the small amplitude limit cycles are either stable or unstable respectively [73]. The large amplitude, relaxation-type limit cycles are always stable. In Figs. 2-A and -B we illustrate the supercritical canard explosion for the FHN model as λ increases from $\lambda = 0.0078$ to $\lambda = 0.0079$. The critical range over which the canard explosion occurs can be approximated by a critical value for the control parameter given in terms of the other model parameters [71] (see also [74]). For the control parameter λ,

$$\lambda_c = \frac{\alpha}{36}\,[\,3+\alpha\,]\,\epsilon + \mathcal{O}(\epsilon^{3/2}). \tag{7}$$

Analogous expressions can be found for the parameter α. Since λ parametrizes the location of the fixed-point of eqs. (1), λ_c defines a critical fixed-point $(\bar{v}_c, \bar{w}_c)$. For fixed-points $(\bar{v}, \bar{w})$ to the left (right) of $(\bar{v}_c, \bar{w}_c)$, system (1) displays SAOs (LAOs). For a technical discussion on the Hopf bifurcation and the canard phenomenon for two-dimensional systems we refer the reader to [75] (Appendix A).

The canard phenomenon is important not only because of the explosion of limit cycles but also because it reflects the way the vector field organizes around the knee of the v-nullcline where this explosion occurs (left knee in Fig. 2) for values of λ close to λ_c. This has significant consequences both for the way in which oscillators respond to external inputs and for network dynamics.

A salient feature of the canard phenomenon, relevant for the mechanisms we describe in this paper, is that for values of λ close enough to λ_c, trajectories are able to evolve in close vicinities of the unstable (middle) branch of the v- nullcline for a significant amount of time before moving either to the left, to generate small amplitude oscillations (SAOs), or to the right, to generate large amplitude oscillations (LAO). Fig 2-D shows two superimposed segments of the limit cycle trajectories presented in Figs. 2-A and -B on a magnified view of the phase-plane. Fig 2-E shows the corresponding v- and w-traces. In a vicinity of the left knee of the v-nullcline trajectories evolve slowly while they "climb up" the unstable branch of the v-nullcline.

For values of λ close to λ_c, these region in phase-plane is very sensitive to small perturbations that can dramatically change the local dynamics from SAOs to LAOs and vice versa. In addition, trajectories starting away from the small amplitude limit cycle pass close to it but do not necessarily converge to it in the "first round" (Fig. 2-F). Instead, they make a whole excursion around the cubic nullcline (not shown) before converging to the small amplitude limit cycle. A transient perturbation of the cubic nullcline, such as the one resulting from the forcing term described in Section 2.3, can switch the limit cycle amplitude regime between SAOs and LAOs.

The ability of trajectories to follow the unstable branch decreases as λ increases, and virtually disappears for large enough values of λ as we illustrate in Fig. 2-C ($\lambda = 0.5$). There, trajectories arriving in the left knee move along the fast direction without following the unstable branch. Once

the trajectory passed the left knee, a stronger perturbation is needed in Fig. 2-C than in Fig. 2-B to produces a SAO instead of a LAO. In the subcritical case, SAO and LAO trajectories are separated by a small amplitude limit cycle (not shown).

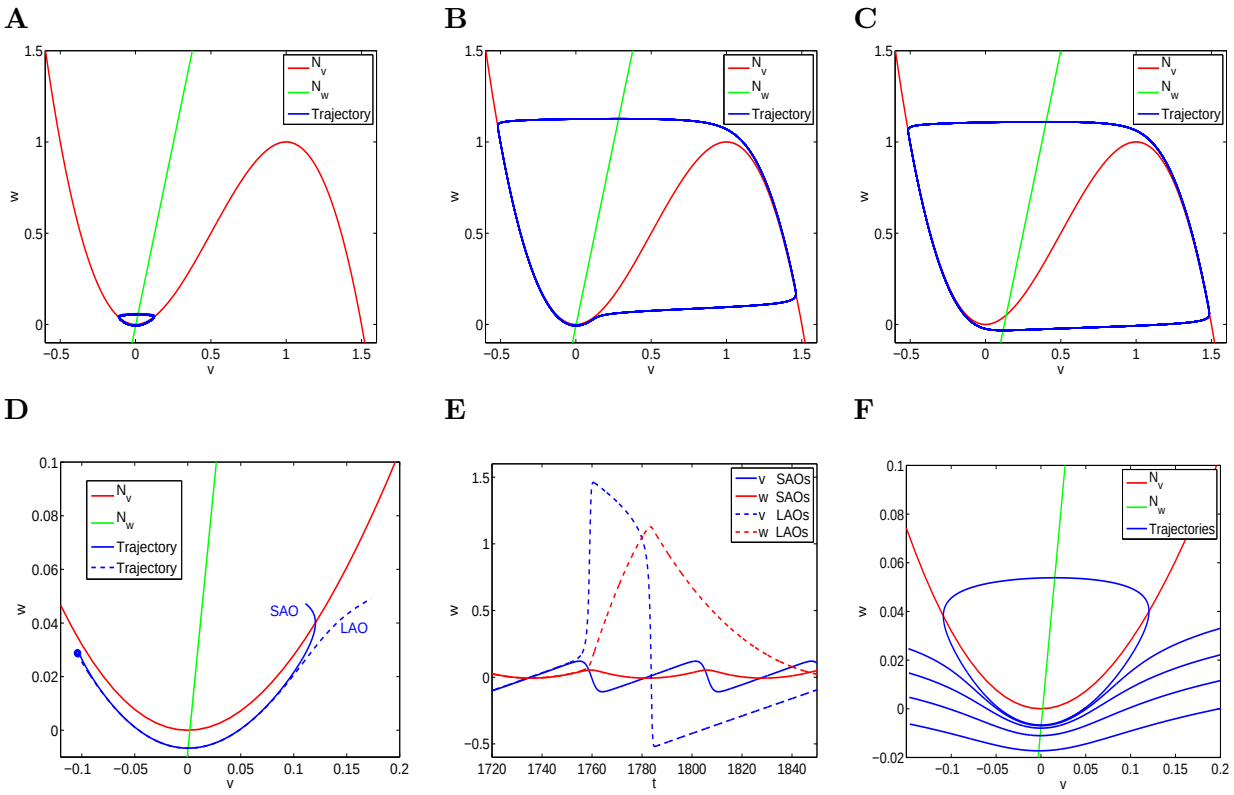

Figure 2: **Supercritical canard explosion of limit cycles for the FHN model for a representative set of parameters. A.** Small amplitude oscillations (SAOs) for $\lambda = 0.0078$. **B.** Large amplitude oscillations (LAOs) for $\lambda = 0.0079$. **C.** LAOs for $\lambda = 0.5$. The curves N_v and N_w represent the v- and w-nullclines respectively. **D.** Superimposed phase-planes for the values of λ in A and B showing segments of the corresponding trajectories. **E.** Superimposed graphs of v and w vs. t for the two trajectories shown in A and B over a LAO period. **F.** SAOs and representative neighboring trajectories for $\lambda = 0.0078$ (as in A). These trajectories jump up and make a LAO before converging to the small amplitude limit cycle. We used the following parameter values: $\epsilon = 0.01$, and $\alpha = 4$.

Although the globally coupled system (5) is four-dimensional, its dynamics can be investigated by looking at two forced two-dimensional systems where each oscillator in (5) is forced by the inhibitor variable (w) of the other one. As we discussed earlier, the effect of these forcing terms is to raise and lower the other oscillator's v-nullcline. This dynamically changes the location of the effective fixed-points thus affecting the local vector field. In some cases, depending on the values of γ, σ_1 and σ_2, it can lead to transient changes from SAOs to LAOs and vice versa.

The canard phenomenon in three-dimensional systems has been studied in [76, 77, 78]. Here we provide a heuristic explanation of how the canard critical value (7) of the autonomous part ($w_j = 0$) of each oscillator in (5) is affected by γ, the cluster sizes (σ_1 and σ_2), and w_j. We consider constant values of w_j and we look at the time-dependent effects of w_j as a sequence of these constant values. Define

$$u_k = (1 + \sigma_k \gamma)\, w_k - \gamma\, w_{tgt} + \gamma\, \sigma_j\, w_j. \tag{8}$$

Differentiating with respect to t, substituting into the second equation in (5) and rearranging terms yields

$$u_k' = \epsilon\, [\, (1 + \sigma_k\gamma)\, \alpha\, v_k - (1 + \sigma_k\gamma)\, \lambda - \gamma w_{tgt} + \gamma\sigma_j w_j - u_k\,]. \tag{9}$$

Calling

$$\hat{\alpha} = (1 + \sigma_k\gamma)\, \alpha \qquad \text{and} \qquad \hat{\lambda} = (1 + \sigma_k\gamma)\, \lambda + \gamma w_{tgt} - \gamma\sigma_j w_j \tag{10}$$

eq. (8) becomes

$$u_k' = \epsilon\, [\, \hat{\alpha}\, v_k - \hat{\lambda} - u_k\,]. \tag{11}$$

This is the same as the second equation in the FHN model of the form (1) where w is substituted by u_k. The corresponding canard critical value is given by [75]

$$\hat{\lambda}_{c,k} = \frac{\hat{\alpha}}{8\, a^3}\, [\, 2\, a^2 + 3\, \hat{\alpha}\, h\,]\, \epsilon + \mathcal{O}(\epsilon^{3/2}). \tag{12}$$

Substituting $\hat{\alpha}$ and $\hat{\lambda}$ in (12) by their expressions given in (10) yields an effective critical value

$$\lambda_{c,k} = \lambda_c + \frac{3\, h\, \alpha^2 \gamma\, \sigma_k}{8\, a^3}\epsilon - \frac{\gamma\, w_{tgt}}{1 + \gamma\sigma_k} + \frac{\gamma\, \sigma_j w_j}{1 + \gamma\sigma_k}. \tag{13}$$

The second and third term in (13) are a "static correction" to the canard critical value for the uncoupled oscillator ($\gamma = 0$) due to the autonomous part ($\sigma_j = 0$) in system (5). The fourth term in (13) is a "dynamic correction" to the canard critical value for oscillator k due to the effect of oscillator j. Changes in the effective canard critical value imply that trajectories that are in the LAO regime for $\gamma = 0$ may be in the SAO regime for $\gamma > 0$ and viceversa. For time-dependent values of w_j, these changes may transiently occur in a time-interval within the oscillation period.

3 Basic mechanisms

Three questions relevant for the understanding of the mechanisms of generation of phase-locked oscillations are (i) How do two oscillators that are initially close enough separate to form phase-locked patterns?, (ii) How is the phase-difference maintained? (stability), and (iii) How close is close enough? (i.e., how does the basin of attraction of phase-locked patterns depend on the model parameters?).

We have identified three qualitatively different basic mechanisms that contribute to answering these questions in the globally coupled FHN model we investigate here. We discuss them below in this Section in the context of the specific example presented in Fig. 3. In Sections 4 and 5 we discuss the role they play in the mechanisms of generation of phase-locked patterns in two-cluster systems with the same and different sizes respectively.

The two patterns in Fig. 3 are qualitatively different. In Fig. 5-A ($\gamma = 0.1$), there is an initial small amplitude oscillation (SAO) in the red oscillator and no noticeable SAOs in the subsequent red cycles nor in the blue oscillator. In Fig. 5-B ($\gamma = 4$) both oscillators show SAOs in all cycles. However, the first SAO in the red oscillator has a larger amplitude (and different shape) than the subsequent ones.

The first red SAO in both panels results from the *swing-and-release* (SR) mechanism which is related to the canard phenomenon (compare the shapes of these initial oscillations and the SAO in Fig. 2-D). The delay in the remaining periods for both oscillators in panel A result from a weak version of the *hold-and-release* (HR) mechanism. The subsequent oscillations in panel B result from a strong version of the HR mechanism.

In what follows we will refer to the oscillators described by the variables (v_1, w_1) and (v_2, w_2) as the "blue" and "red" oscillators respectively, and we will use a similar terminology for their corresponding cubic v-nullclines $N_{v,1}$ and $N_{v,2}$.

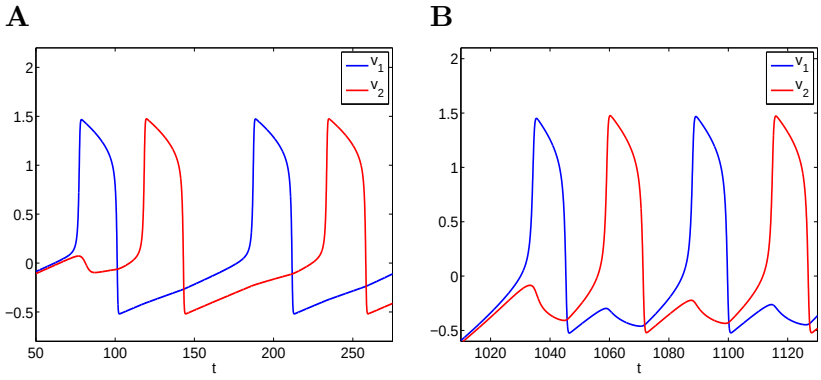

Figure 3: **Generation of antiphase patterns in the globally coupled FHN model for two representative values of γ.** In both cases the two oscillators were connected at $t = 0$. Before this time the (uncoupled) oscillators were active for 1000 units of time and had reached steady LAOs. In both cases, these patterns approach antiphase as time increases. We used the following parameter values: $\alpha = 4$, $\epsilon = 0.01$, $\lambda = 0.01$, $\sigma_1 = \sigma_2 = 0.5$. **A.** $\gamma = 0.1$. **B.** $\gamma = 4$.

3.1 Swing-and-release (SR) mechanism

In Fig. 4 we show two snapshots of the phase-planes for the red oscillator in Fig. 3-A for representative values of t during the first cycle. For reference, we also include the blue nullcline and the blue oscillator when it evolves in the region captured by the snapshots. Panel A corresponds to the initial time in Fig. 3-A. The dotted red curve describes the trajectory of the red oscillator (red dot) during this cycle until it jumps up. Its dynamics results from both its intrinsic properties and the forcing exerted on it by the blue oscillator (blue dot) through changes in the red nullcline (described in more detail in Section 4).

The two oscillators move around the left knee in a canard-like manner (i.e., spending a significant amount of time moving in a vicinity of the unstable branch of the v-nullcline). The blue oscillator jumps up at $t \sim 70$ (not shown) and lowers the red nullcline (because w_1 increases). In the absence of any forcing, the red oscillator would also jump up, following the blue oscillator. However, the position of the red oscillator relative to the red nullcline has changed and, instead of jumping up, it crosses the red nullcline, reverses direcion and makes a full oscillation (panel B) before jumping up (panel C). This shows that the initial SAO in Fig. 4-A is a canard-like SAO.

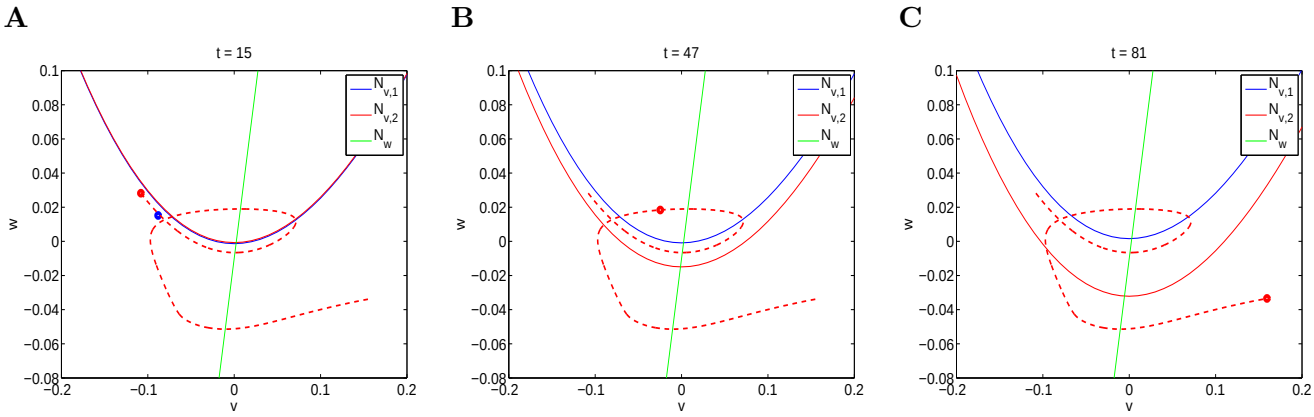

Figure 4: **Swing-and-release (SR) mechanism.** Snapshots of the phase-plane for the first cycle in Fig. 3-A. In panel A the the red and blue nullcline are almost superimposed since the distance between the two oscillators in phase-plane is very small. We used the following parameter values: $\alpha = 4$, $\epsilon = 0.01$, $\lambda = 0.01$, $\gamma = 0.1$, $\sigma_1 = \sigma_2 = 0.5$.

3.2 Weak hold-and-release (wHR) mechanism

The dynamics of the subsequent cycles in Fig. 3-A (that show no SAOs) are governed by the mechanism illustrated in Fig. 5. We show snapshots of the phase-plane for the second red cycle in Fig. 3-A. The blue oscillator is evolving along the right branch of the blue nullcline (not shown). Its dynamics affects the location of the red nullcline that first shifts down, holding the red oscillator (panel B), and

then raises, releasing it to jump up. As a, the red oscillator spends a longer time moving along the left branch of the red nullcline than it would in the absence of any coupling. The red oscillator is released before reaching the unstable (middle) branch of the red nullcline (not shown), and then it is not "captured" by this unstable branch in a canard-like SAO.

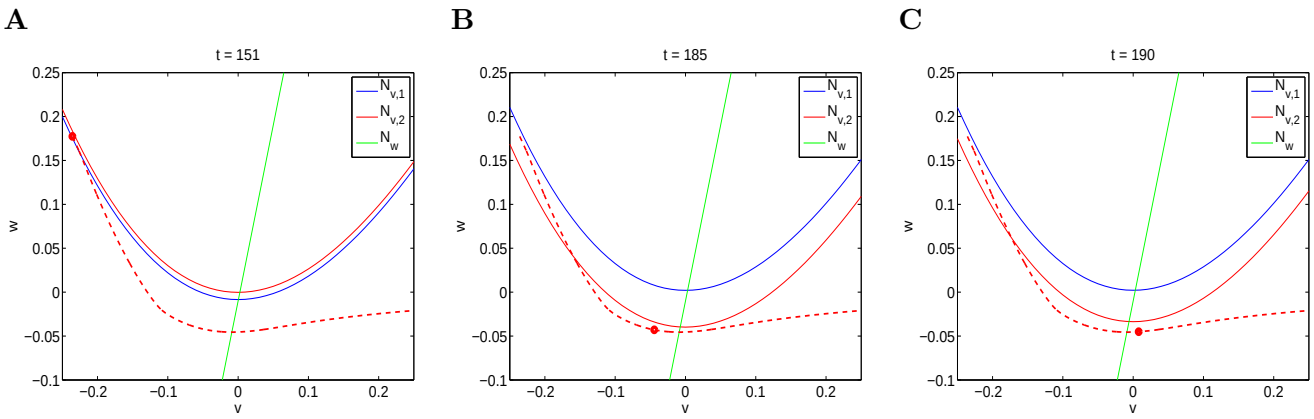

Figure 5: **Weak hold-and-release (wHR) mechanism.** Snapshots of the phase-plane for the second cycle in Fig. 3-A. We used the following parameter values: $\alpha = 4$, $\epsilon = 0.01$, $\lambda = 0.01$, $\gamma = 0.1$, $\sigma_1 = \sigma_2 = 0.5$.

3.3 Strong hold-and-release (sHR) mechanism

Fig. 6 shows snapshots of the phase plane for representative times in the second "red" cycle in Fig. 3-B. For reference, we also show both the blue oscillator and blue nullcline. The red nullcline shifts down in response to the motion of the blue oscillator after it jumps up (not shown). Due to the larger value of γ, the red nullcline shifts down a significantly longer distance than in Fig. 5. As a result, the red oscillator does not only experience a delay but also a transient retraction responsible for second SAO in Fig. 3-B (and the subsequent ones, not shown here). Importantly, the SAO generated by this dynamics is qualitatively different from the canard-like one described in Fig. 4 (wSR).

3.4 Hold-and-escape (HE) mechanism

This mechanism describes the ability of an oscillator (red, say) to jump up while receiving inhibition from the other oscillator (blue, say) while the latter still in its increasing phase (i.e., before the other oscillator reached the right knee of the blue nullcline). The trajectory looks similar to the one for the wHR mechanism. The main difference lies in the relative location of the cubic nullclines along the evolution of the system.

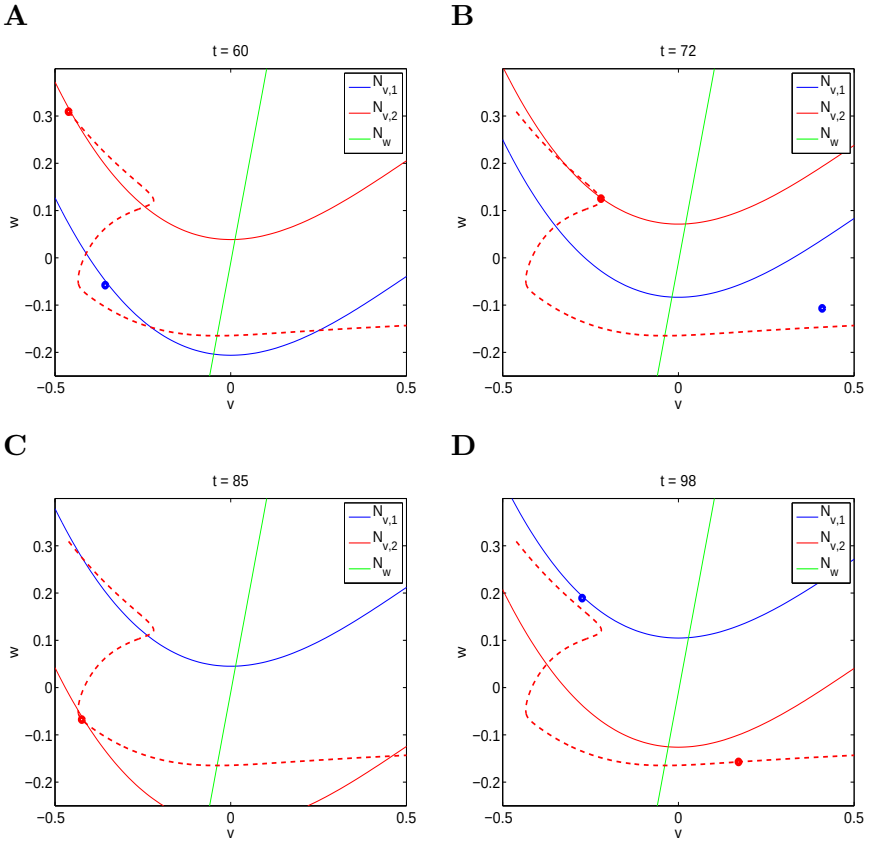

Figure 6: **Strong hold-and-release (sHR) mechanism.** Snapshots of the phase-plane for the second cycle in Fig. 3-B. We used the following parameter values: $\alpha = 4$, $\epsilon = 0.01$, $\lambda = 0.01$, $\gamma = 4$, $\sigma_1 = \sigma_2 = 0.5$.

3.5 Phase separation and jumps

Here we provide a heuristic argument showing that if two oscillators evolving according to eqs. (5) are moving along the same branch (either left or right) of their corresponding v-nullclines, their phase difference either decreases or remains small, and hence phase separation is not likely to occur in these regions. In fact, for phase separation to occur, an extra mechanism such as the ones described above, involving the relative motion of v-nullclines, is needed.

We first consider two trajectories initially located in a small vicinity of either the left or right branches of the v-nullclines $N_{v,1}$ and $N_{v,2}$ (red and blue circles in Fig. 7-A). From (5), the evolution of V and W defined as

$$V = v_2 - v_1 \qquad \text{and} \qquad W = w_2 - w_1 \tag{14}$$

is given by

$$\begin{cases} V' = f(v_2) - f(v_1) - W, \\ W' = \epsilon\,[\,\alpha\, V - W]. \end{cases} \tag{15}$$

From the mean-value theorem, there exists an intermediate value of V^* such that $f(v_2) - f(v_1) = \eta\,(v_2 - v_1)$ where $\eta = f'(V^*) < 0$. For two oscillators initially close enough, η can be approximated by $\eta(V)$ with $\eta(0) = 0$. Eqs. (15) become

$$\begin{cases} V' = \eta(V)\, V - W, \\ W' = \epsilon\,[\,\alpha\, V - W]. \end{cases} \tag{16}$$

The fixed-point for system (16) is $(V, W) = (0, 0)$. A heuristic explanation of the stability properties can be provided in terms of the linear system obtained by considering constant values of η within some appropriate range. The eigenvalues are given by

$$r_{1,2} = \frac{\eta - \epsilon \pm \sqrt{(\eta+\epsilon)^2 - 4\,\epsilon\,\alpha}}{2}. \tag{17}$$

The fixed-point is a focus if $-\epsilon - 2\sqrt{\epsilon\alpha} < \eta < -\epsilon + 2\sqrt{\epsilon\alpha}$ and a node otherwise. A necessary condition for the existence of a focus is that $\epsilon\,\alpha > 0$ which is always satisfied. Foci are stable if $\eta < \epsilon$ and unstable if $\eta > \epsilon$. Nodes are stable if $\eta - \epsilon < 0$ and $\epsilon\,(\eta - \alpha) < 0$ and unstable if either $\eta - \epsilon > 0$ and $\epsilon\,(\eta - \alpha) < 0$ (2 positive eigenvalues) or $\epsilon\,(\eta - \alpha) > 0$ (saddle node) [1]. Since $\epsilon > 0$ and $\alpha > 0$, and $\eta < 0$ on both the left and right branches of the v-nullcline, the fixed-point $(0, 0)$ is stable. Two trajectories initially close enough in a vicinity of these branches of the v-nullcline approach each other. We illustrate this in Fig. 7-A. An important aspect to take into account is that the stability of the fixed-point $(0, 0)$ does necessarily implies monotonic decrease of (V, W) to $(0, 0)$ since damped oscillations are posible when η is sufficiently small (close enough to the knee). Even when $(0, 0)$ is a stable node, an initial oscillation may occur before the trajectory converges to $(0, 0)$. The phase difference of the two oscillators may then slightly increase before decreasing.

If the two oscillators are both located either below or above the middle branch of the v-nullcline ($\eta > 0$) and if $\eta > \epsilon$, then the fixed-point $(0, 0)$ is unstable and the trajectories separate from each other. We illustrate this in Fig. 7-B. As the oscillators move away from the minimum of the v-nullcline, the slope of its middle branch, and possibly also η, increases and one of the trajectories moves fast towards the right branch of the v-nullcline while the other evolves slower in the vicinity of its minimum. This provides the window of opportunity for the mechanisms discussed above to come into play. Note that for this to happens ϵ has to be small enough. For larger values of ϵ, the fixed-point may be stable and the phase difference will stay bounded, and possibly decrease. Note also that the values of λ play no role in the argument discussed here.

[1] These conditions result from the following arguments: (i) If $\eta - \epsilon + \sqrt{(\eta+\epsilon)^2 - 4\alpha\epsilon} < 0$, then $\eta - \epsilon - \sqrt{(\eta+\epsilon)^2 - 4\alpha\epsilon} < 0$. For $\eta - \epsilon + \sqrt{(\eta+\epsilon)^2 - 4\alpha\epsilon} < 0$, $\eta - \epsilon < 0$ and $\epsilon(\eta - \alpha) < 0$, and (ii) If $\eta - \epsilon - \sqrt{(\eta+\epsilon)^2 - 4\alpha\epsilon} > 0$, then $\eta - \epsilon + \sqrt{(\eta+\epsilon)^2 - 4\alpha\epsilon} > 0$. For $\eta - \epsilon - \sqrt{(\eta+\epsilon)^2 - 4\alpha\epsilon} > 0$, $\eta - \epsilon > 0$ and $\epsilon(\eta - \alpha) < 0$.

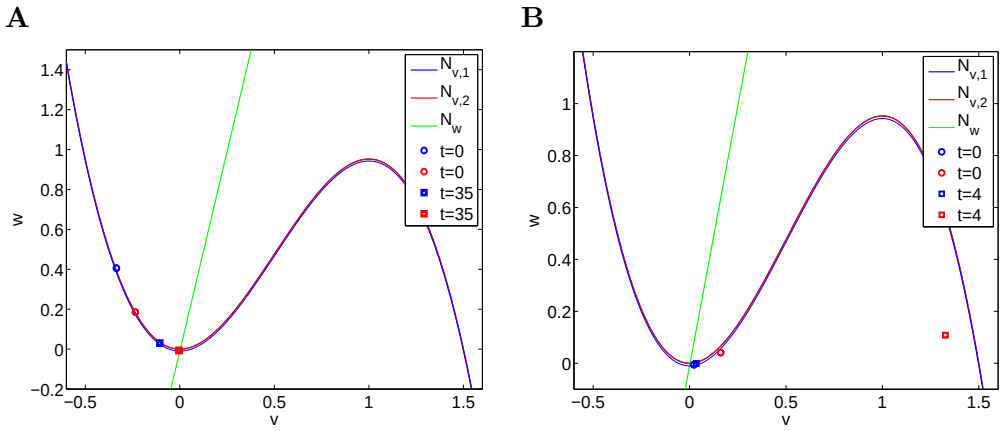

Figure 7: **A. Trajectories initially in a vicinity of the left branch of the v-nullclines ($N_{v,1}$ and $N_{v,2}$) approache each other at time increases.** The cubic nullclines $N_{v,1}$ and $N_{v,2}$ correspond to $t = 0$. **B. Trajectories with initial v-coordinates corresponding to the middle branch of the v-nullclines separate from each other as time increases**. $N_{v,1}$ and $N_{v,2}$ correspond to $t = 0$ in panel **A**. Note that the blue oscillators is located almost at the same point for $t = 0$ and $t = 4$. We used the following parameter values: $\alpha = 4$, $\epsilon = 0.01$, $\lambda = 0.01$, $\gamma = 0.1$, $\sigma_1 = \sigma_2 = 0.5$.

4 Two-cluster systems with the same cluster size

Here we consider system (5) with $\sigma_1 = \sigma_2 = 0.5$, $\epsilon = 0.01$, and various representative values of λ and the global feedback parameter γ. Our results are presented in Fig. 8. We considered some specific cases in our discussion of the basic mechanisms in Section 3.

We measure the phase difference between two oscillators (from now on the "phase") as the absolute value of the time difference between two consecutive peaks in the graphs of v_1 and v_2 divided by their oscillation period (which is the same for both oscillators). The phase prior to the "connection" time ($t = 1000$) reflects the initial phase.

For small enough values of λ we found only antiphase patterns. As λ increases, synchronized (in phase) patterns emerge with a basin of attraction smaller than the one for antiphase patterns. For large enough values of λ we also found out-of-phase (not antiphase) patterns.

4.1 SR and wHR mechanisms govern the generation of phase-locked cluster patterns for small values of λ

Fig. 8-A shows the antiphase patterns for $\lambda = 0.01$ and $\gamma = 0.1$. (These are the same parameters used in Fig. 3 for the two first cycles). In Fig. 8-A, the initial phase is very small. Phase separation occurs in the first cycle after connection time by the SR mechanism discussed in Section 3.1 (see Fig. 4). The antiphase pattern is maintained by a weak HR mechanism discussed in Section 3.2 (see Fig.

5).

In Fig. 9 we illustrate the evolution of the two oscillators in phase-space. The first two panels (top-left and top-middle) show the full trajectories of the two oscillators respectively during the first cycle after they were connected. For reference, we present a nullcline for a representative value of t. The red oscillator displays a canard-like SAO follow by a LAO (SR and wHR mechanisms). The blue oscillator displays only a LAO (wHR mechanism).

The remaining panels show snapshots of the evolution of the two oscillators and their respective nullclines. Initially, the two oscillators are on the left branch of their v- nullclines which are almost superimposed ($w_1 \sim w_2$). During phase separation (SR mechanism) the blue oscillator jumps up, lowering the red nullcline, it climbs up the blue nullcline, and subsequently jumps down, releasing the red oscillator. When the red oscillator jumps up it lowers the blue nullcline, holding the blue oscillator. This delays the jumping up of the blue oscillator (wHR). After the red oscillator jumps down, the blue nullcline raises, the blue oscillator is released (jumps up), and the cycle starts again. Note that the existence of the antiphase solution does not require that oscillators be in different branches of their v-nullclines (jumping up and down at the same time). In fact, Figs. 9 shows that the two oscillators coexist in the left branch for a significant amount of time (see $t = 110$ for instance). For two oscillators initially well separated, the wHR mechanism is responsible for the stabilization of the antiphase patterns.

4.2 HE and wHR mechanisms govern the generation of phase-locked cluster patterns for large values of λ

Fig. 8-D shows that for larger values of λ phase separation is less abrupt. As λ increases it takes a larger number of periods for the system to reach the antiphase regime. For $\lambda = 0.5$ (Fig. 8-B), for instance, the oscillators slowly drift apart from their initial phase to stabilize in an antiphase pattern (Fig. 8-C, left) with no initial canard-like SAO. The mechanism by which phase separation occurs involves the HE and weak HR mechanisms. Soon after the two oscillators are coupled the red oscillator reaches the left knee of the red nullcline (escaping) during the rising phase of the blue oscillator (before the blue oscillator reaches the right knee). As it moves around the left knee of the red nullcline, the red oscillator slows down, and consequently the phase slightly increases. After jumping up, the red oscillator climbs up the right branch of the red nullcline. The corresponding increasing value of w_2 lowers the blue nullcline. This facilitates the jumping down of the blue oscillator (which was still moving along the right branch of the blue nullcline), thus increasing the phase further. Subsequently, the motion of the blue oscillator along the left branch of the blue nullcline raises the red nullcline (that had previously shifted down due to the high value of w_1 near the right knee). As the phase increases, the HE mechanism slowly transitions into a wHR mechanism responsible for maintaining the antiphase pattern.

The switch from a SR to a HE/wHR mechanism as λ increases (for fixed-values of γ) is the result of λ being further away from λ_c. Similarly to what occurs in Fig. 2-C, for these relatively large values of λ, trajectories arriving in a vicinity of the left knee are in a LAO regime and have lost the ability of crossing the middle branch of their v-nullclines; i.e., have lost the ability to generate canard-like

SAOs.

4.3 A wHR mechanism and the slow rise time of the inhibitor are responsible for the generation of in-phase patterns for large values of λ

For $\lambda = 0.01$ we didn't find stable in-phase-patterns. Fig. 8-E shows that if they exist, their basin of attraction is extremely small. This panel also shows that as λ increases, there is bistability between in-phase and out-of-phase patterns. The size of the basin of attraction for in-phase patterns increases with λ. Note that for $\lambda = 1.5$ the out-of-phase patterns are phase-locked but not antiphase (see also Fig. 8-C, right panel). Comparison between Figs. 8-E ($\gamma = 0.1$) and 8-F ($\gamma = 2$) illustrates that the transition from the initial phase to either in-phase or phase-locked patterns is more abrupt as γ increases.

The mechanism of in-phase synchronization of two globally coupled oscillators initially close enough involves the wHR mechanism and the relatively slow rise time of the inhibitory variables (w_1 and w_2). We illustrate this in Fig. 10 for $\lambda = 1.5$ and $\gamma = 2$. When the two oscillators move down along the left branch of their v-nullclines, their w-values decrease, raising each others cubic nullclines, and allowing the two oscillators to jump without stretching their distance. Specifically, after the first (blue) oscillator jumps up, w_1 starts increasing. However, the small rise time of w_1 as compared to v_1 (see Fig. 2-E) causes a slow shift down of the red nullcline that is not strong enough so as to prevent the red oscillator from jumping up, following closely the blue oscillator without creating any significant delay (and without generating any canard-like SAO). This effect is strongly dependent on the fact that λ is large enough so limit cycle trajectories do not follow the unstable branch of the cubic nullcline (see Fig. 2-C). This is different from what occurs for smaller values of λ for which limit cycle trajectories do follow the unstable branch for a significant amount of time (see Fig. 2-B) and cause a phase separation by the SR mechanism. In these cases, a small increase in w_1 is enough for the red oscillator to be "captured" inside the cubic nullcline and forced to reverse direction.

In-phase synchronization is the result of successive contractions. In Fig. 10, the blue oscillator jumps up first but the red oscillator jumps up at a "higher height" (higher value of w_2), leading to a contraction in the distance between the two oscillators. They continue to evolve, closer than in the silent phase, with the consequent reduction in the difference between the heights of both nullclines. Another contraction occurs when the two oscillators jump down. The blue oscillator jumps down first but the red oscillator jumps down from a "lower height" (lower level of w_2) arriving roughly to the same point in the corresponding left branches of the v-nullclines roughly at the same time.

4.4 The oscillation frequency increases with increasing values of the global coupling parameter γ

In Fig. 11-A we compare the antiphase patterns for values of γ increasing from left to right. All other parameters are as in Fig. 8. As γ increases the oscillation period decreases (see also Fig. 11-C) and

the SAOs in the mixed-mode oscillatory antiphase patterns are more prominent. As discussed above, phase separation is governed by the SR mechanism. For low values of γ the trajectory is released after the swing. For larger values of γ the trajectory is first hold and then released thus increasing the size of the first SAO. The subsequent SAOs result from a HR mechanism that transition from weaker to stronger as γ increases. For larger values of λ (Fig. 11-B) the dependence of the oscillation period on γ is less pronounced (Fig. 11-C). The increase in oscillation frequency as γ increases results from the reduction in the distance between the two knees of the v-nullclines. Note that this increase in frequency as γ increases is counter-intuitive in the sense that is caused by global inhibition. Note also the qualitative differences between the patterns for both values of λ.

5 Two-cluster systems with different cluster sizes

Here we consider system (5) with $\sigma_1 = 0.2$, $\sigma_2 = 0.8$, $\epsilon = 0.01$, and various representative values of λ and the global feedback parameter γ. The choice of σ_1 and σ_2 is representative for clusters of different size. We call $\Delta\sigma = |\sigma_2 - \sigma_1|$. In Fig. 12 we show the results of our simulations for a representative set of parameters.

There are some important differences between the patterns obtained for different (Fig. 12, $\sigma_1 = 0.2$ and $\sigma_2 = 0.8$) and same (Section 4, $\sigma_1 = \sigma_2 = 0.5$) cluster sizes. First, although in both cases, the phase-locked clusters display mixed-mode oscillations, the SAOs are qualitatively different for both oscillators (Fig. 12-A) in the heterogeneous case. In particular, they are lower in the blue oscillator than in the red oscillator. We explain the mechanisms underlying these differences below. Second, for $\Delta\sigma$ large enough, M:1 patterns, consisting of M red LAOs per cycle, emerge. For the parameters in Fig. 12, $M = 1, \ldots, 3$. In other parameter regimes, the number of red LAOs per cycle can be larger (e.g., $\alpha = 2$, $\lambda = 0.04$, $\gamma = 40$, $M = 6$). In all cases, the blue SAOs builds up while receiving pulses of inhibition from the red LAOs until the blue oscillator is able to overcome this inhibition. Third, in 1:1 oscillatory patterns, both the period and phase depend on $\Delta\sigma$. The larger $\Delta\sigma$, the smaller the phase and the smaller the period (Fig. 13-A). Fig. 13-A also shows that the period decreases with increasing values of γ. The reduction of the period with increasing values of γ and the cluster size difference ($\Delta\sigma$) results, primarily, from the flatter shape of the "autonomous part" (first term) of the v-nullcline 6. Finally, synchronized (in-phase) oscillations are favored for larger values of $\Delta\sigma$.

In Figs. 13-B and -C we show the phase of two clusters with $\sigma_1 = 0.2$ ($\Delta\sigma = 0.6$) and various representative values of λ for $\gamma = 0.1$ and $\gamma = 1$ respectively. The remaining parameters are as for $\Delta\sigma = 0$ (Fig. 8-E). While for $\Delta\sigma = 0$ and $\lambda = 0.5$, the globally coupled system is bistable, we have found no bistability for $\Delta\sigma = 0.6$ and $\lambda = 0.5$ (if it exists, its basin of attraction is very small). Note that, contrary to intuition, the break of symmetry in the cluster sizes favors the generation of in-phase synchronized clusters.

5.1 HR and SR mechanisms govern the generation of 1:1 patterns for small values of λ

The mechanism of generation 1:1 phase-locked patterns is heterogeneous and involves a combination of the HR (blue oscillator) and SR (red oscillator) mechanisms. The former gives rise to the lower SAOs in the blue oscillator and the latter gives rise to the higher SAOs in the red oscillator. A more detailed description of the dynamics in terms of the geometry of the phase-space is presented in Fig. 14. We start with the two oscillators in the silent phase (top panels). During this phase, the two oscillators evolve closer together than for $\Delta\sigma = 0$. The blue oscillator jumps up, lowering the red nullcline, and causes the red oscillator to swing (SR mechanism). While the red oscillator is still moving around the left knee, the blue oscillator jumps down, rising the red nullcline, and releasing the red oscillator that jumps up. As the red oscillator climbs up the red nullcline, it lowers the blue nullcline, holding the blue oscillator. This allows the red oscillator to jump down and arrive in a vicinity of the blue oscillator, thus closing the cycle.

Geometrically, the cluster size difference is reflected in differences in the shapes of the v-nullclines (6) and differences in the forcing effects each oscillator exerts on the other. The larger the cluster size, the flatter the "autonomous" part (first term) of the v-nullcline (6). In Fig. 12, the flatter v-nullclines for $\sigma = 0.8$ is reflected in the flatter limit cycles for the red oscillator. The non-autonomous part is affected by the cluster size of both oscillators. Differences in cluster size also create differences in the effective canard critical values for both oscillators (13). For small enough values of w_{tgt} (as the ones we consider here) and fixed values of γ, the larger the cluster size, the larger $\lambda_{c,k}$; i..e, for a fixed-value of λ, the tendency of trajectories to display canard-like SAOs increases with cluster size. The number of red peaks per cycle increases with γ. For larger values of γ the globally coupled system displays synchronized SAOs (not shown).

5.2 HR and SR mechanisms govern the generation of M:1 patterns for small values of λ

The mechanism of generation of 2:1 LAO patterns (Figs. 12-B) involves a HR (red and blue oscillators) and a SR (blue oscillator) mechanisms. (Note that the roles of both mechanisms are different than for 1:1 patterns.) The HR mechanism gives raise to the SAO (below the blue LAO) and the lower blue SAO. The SR mechanism gives rise to the large blue LAO. In Fig. 15 we present snapshots of the evolution of the two oscillators for representative values of t.

Again, we start with the two oscillators in the silent phase (top panels). In contrast to the previous case (Fig. 14), the red oscillator is now preceding the blue oscillator. (We explain the reason for that at the end of the paragraph.) As they evolve, their nullclines raise. When the two oscillators arrive to the left knee, the red oscillator jumps up and slightly lowers the blue nullcline. This causes the blue oscillator to swing (canard-like SAO) while the red oscillator is climbing up the red nullcline. After the red oscillator jumps down it shifts down the red nullcline, rising the blue nullcline, and eventually releasing the blue oscillator which jumps up. Note that during this intermediate interval of time where the two oscilators are in the silent phase, the blue oscillator is preceding the red oscillator, differently

than at the beginning (and end) of the cycle. As the blue oscillator moves along the blue nullcline, w_1 increases and the red nullcline shifts down holding red oscillator which is released after the blue oscillator jumps down. The increase in w_2 as the red oscillator moves along the red nullcline shifts down the blue nullcline and holds the blue oscillator. When the red oscillator jumps down, w_2 (red oscillator) is lower than w_1 (blue oscillator) and so the red oscillator jumps down and overtakes the blue oscillator who is left slightly behind. (This explains the initial panel in Fig. 15.)

M:1 patterns are not restricted to these shown in Fig. 12. For instance, there is a 2:1 pattern for $\gamma = 2$ with a red SAO (in between Figs. Fig. 12-A and -B) and a 2:1 pattern with two red SAOs for $\gamma = 8$ (in between Figs. 12-B and C). In both cases, these SAOs are generated by a SR mechanism. In the former case, due to the additional SAO, the red oscillator is overtaken by the blue oscillator on the silent phase as it occurs for $\gamma = 2$. In the latter case, the two oscillators make a simultaneous swing after which the blue oscillator is released and the red oscillator if forced to make a second swing before being released. For the 3:1 pattern in Fig. 12-E ($\gamma = 15$), the red SAO results from a SR mechanism while the three blue SAOs result from HR mechanisms.

6 Discussion

We have studied the mechanism of generation of in-phase and phase-locked oscillatory patterns in a two-cluster system of globally coupled, fast-slow FHN oscillators where the activator (v) receives global feedback from the inhibitor (w), mimicking the type of global feedback used for the BZ reaction with photochemical global feedback investigated in [10, 11, 12, 13]. Globally coupled FHN oscillators have been studied before [61, 59]. However, in these works the activator receives global feedback from the activator rather than the inhibitor. The prototypical example is a global feedback term of the form (4).

Previous theoretical studies on globally coupled FHN oscillators (and other oscillators of FHN type) have been based mainly on numerical simulations and bifurcation analysis. In this paper, we incorporated the use of dynamical systems tools to investigate the role of the relevant parameters in the generation of the patterns mentioned above. These are the global coupling parameter γ, the cluster sizes σ_1 and σ_2 ($\sigma_1 + \sigma_2 = 1$), and λ, that controls the location of the fixed-point $(\bar{v}, \bar{w})$. For $\lambda = 0$ the fixed-point coincides with the minimum $(0, 0)$ of the cubic nullcline. Detailed mechanistic studies of phase-locked and in-phase oscillations using dynamical systems tools have been pursued in synaptically coupled neural system under certain assumptions [32, 56, 57, 79, 80] (see also [58, 64]).

For equal-size clusters ($\Delta\sigma = 0$), the prevailing phase-locked patterns are antiphase. For $\lambda = 0.01$ we did not find in-phase patterns. For larger values of λ there is bistability. The basin of attraction of in-phase patterns is much smaller than the basin of attraction of phase-locked patterns (Fig. 8) and it increases with increasing values of λ. We did not find in-phase patterns as the only phase attractor. An increase in the value of γ makes the transition from an initial phase to the steady (in-phase or phase-locked) patterns significantly more abrupt, and it slightly increases the basin of attraction of in-phase patterns for large enough values of λ.

For clusters with different sizes ($\Delta\sigma > 0$), phase-locked patterns are not antiphase (see Fig. 13).

The steady phase changes monotonically with the cluster size difference $\Delta\sigma$. In contrast to the homogeneous case ($\Delta\sigma = 0$), the steady phase in phase-locked patterns depends on γ. (The phase for $\Delta\sigma = 0$ and $\lambda = 1.5$ in Fig. 8-E is an outlier.) The break of symmetry in the cluster sizes $\Delta\sigma > 0$) favors in-phase synchronization rather than phase-locking. Specifically, the range of values of λ for which there is bistability decreases with increasing values of $\Delta\sigma$ while the ranges of values of λ for which only in-phase patterns occur increase. Also, the range of values of λ for which only phase-locked patterns exist slightly increases.

We have identified three basic mechanisms that contribute to the generation of the observed patterns. The swing-and-release (SR) mechanism is related to the canard phenomenon and operates for small values of λ ($\lambda > 0$) that are close enough to the effective canard critical value $\lambda_{c,k}$ (13); i.e., for fixed-points that are close enough to the minimum of the cubic nullcline. Phase separation occurs because while the first oscillator (blue) is able to jump up without significant delay, the second one (red) is "caught" in a canard-like SAO before jumping up. The slight shifting down of the red nullcline caused by the blue oscillator in his way up (along the blue nullcline) is enough to leave the red oscillator in the SAO regime. Central to this is the ability of trajectories to follow the unstable branch of the cubic nullcline for a significant amount of time, a canard related feature. An increase in the value of γ produces the combined effect of increasing the effective canard critical value, making it possible for a system with larger values of λ to display SAOs, and shifting the nullclines down to lower values as the result of the forcing exerted by the other oscillator. This causes the observed faster phase separation and larger initial red SAO.

For values of λ away from λ_c, trajectories loose the ability to follow the unstable branch of the cubic nullcline and instead move in more horizontal, fast, directions. This combined with the slow rise time of the inhibitor as compared to the activator causes two oscillators with an initially small enough phase (below some threshold) to jump up almost at the same time with no canard-like delay for the red oscillator. The sequence of time contractions that occur at each jump lead to in-phase synchronization. For initial phases above that threshold a slow phase drift, rather than a canard-like SAO, leads to phase-locked patterns. The delay associated with this drift is created by the hold-and-escape (HE) and hold-and-release (HR) mechanisms. For intermediate values of λ a combination of SR and HR/HE mechanisms is responsible for the generation of phase-locked patterns. More specifically, as λ the SR mechanism transitions to the wHR mechanism.

For large enough values of γ, phase-locked patterns consist of mixed-mode oscillations (MMOs) where LAOs coexist with SAOs (see Fig. 11). For $\Delta\sigma = 0$ (clusters with equal size), SAOs are created by a strong SR mechanism; i.e., they are canard-like SAOs. As γ increases, after making a full canard-like oscillation, trajectories follow the motion of their corresponding cubic nullclines to reach lower values of v thus generating SAOs with larger amplitude. For $\Delta\sigma > 0$ (clusters with different size), the SAOs in 1:1 patterns are generated by different mechanisms: strong HR for the smaller cluster and SR for the larger cluster (see Fig. 12-A). This persists for M:1 patterns ($M > 1$) obtained for larger values of γ with some exceptions for these values of γ close to the transitions from M:1 to M+1:1 patterns (e.g., see Fig. 12-B) where irregularities occur. We did not analyzed these irregular patterns in this paper.

The HR and HE mechanisms are related to the release and escape mechanisms described for

synaptically connected neural models via fast threshold modulation (FTM) [56, 57, 58, 81]. In FTM, the forcing that each oscillator exerts on the other is fast and has no inherent dynamics. When one oscillator crosses a threshold value, it instantaneously raises or lowers the v-nullcline of the other with a change of shape. If the coupling is inhibitory, a jump up lowers the v-nullcline and a jump down raises it back to its original position. Trajectories react to the instantaneous motion of these nullclines. Intrinsic escape occurs if the oscillator in the silent phase reaches the left knee before the other oscillator jumped down. Intrinsic release occurs if the oscillator in the active phase jumps down before the other oscillator reached the left knee thus releasing it from inhibition. This assumes that threshold lies in the middle branch region of the cubic nullcline [56]. Synaptic escape and release occurs when threshold is in the left and right regions of the cubic nullcline respectively [57].

Similarly to FTM, as the result of global coupling the cubic nullclines raise and shift down with a change of shape. The global coupling we consider in this paper has two terms (6), one that affects each oscillator's intrinsic dynamics (changes the shape of the v-nullcline) and the other that exerts an external forcing (raises and lowers the v-nullcline) of one oscillator onto the other. In contrast to FTM, the forcing term has intrinsic dynamics given by the raising and decay times of the inhibitor. This time scales are translated into the dynamics (shifting down and raising respectively) of the v-nullclines. Trajectories and cubic nullclines move simultaneously and, in many cases, trajectories are "held" by the nullclines in their evolution as it occurs in the SR and HR mechanisms (see Figs. 4, 5 and and 6).

In this paper we have not presented results on the effects of changes in the parameters α and ϵ. Since α governs the slope of the w-nullcline, quantitative changes are expected in the values of the period, phase, and the boundaries between different types of solutions but not qualitative mechanistic differences are expected for values of α within some $\mathcal{O}(1)$ range. Numerical simulations not presented here support this claim. One important consequence of the reduction in the value of α is that it may switch the Hopf bifurcation, and consequently the canard phenomenon, from supercritical to subcritical in the uncoupled cells. However, the canard-related SR mechanism is not dependent on the type of criticality of the canard phenomenon but rather on the ability of trajectories to generate SAOs (either sustained or damped) which occur in the subcritical case. On the other hand, the SR mechanism is strongly dependent on the fact that the system is fast-slow ($0 < \epsilon \ll 1$). Our conclusions are expected to hold for some larger range of values of ϵ than the one considered here. The type of patterns obtained for values of ϵ outside this regime and the mechanisms that give rise to these patterns call for more research.

In this paper, we focused on the mechanisms of generation of two-cluster patterns by assuming the set of individual oscillators initially divided into two clusters oscillating out-of-phase but not on the mechanism by which these individual oscillators are grouped into clusters. More research is needed to understand the underlying mechanisms and to determine how the selection of cluster sizes depends on the model parameters. Additional research is needed to understand how individual oscillators are spatially grouped into clusters in spatially extended systems where diffusion may play a significant role, and what is the effect of small random deviations from perfect synchrony that may be present in a more realistic cluster on the mechanism of generation of phase-locked cluster patterns.

The model we studied in this paper is motivated by previous studies on the BZ reaction with pho-

tochemical global feedback [10, 11, 12, 13]. The FHN system is a caricature model of the Oregonator and other biologically and biochemically realistic models [3, 4]. The mechanisms uncovered in this paper are expected to be also present in the globally coupled Oregonator [11] and modified Oregonator models [12] as well as in other globally coupled oscillatory models [17]. However, the extent to which this occurs and the dependence on chemical (physical, biological, etc) parameters calls for more research.

Acknowledgments

This work was partially supported by the National Science Foundation grant DMS-0817241 (HGR). We thank A. Bose and F. Nadim for useful discussions and comments on this paper.

References

[1] S. H. Strogatz. *Nonlinear Dynamics and Chaos*. Addison Wesley, Reading MA, 1994.

[2] F. Sagués and I. R. Epstein. Nonlinear chemical dynamics. *Dalton Trans.*, pages 1201–1217, 2003.

[3] J. D. Murray. *Mathematical Biology: I. An Introduction*. Springer, Berlin, 2002.

[4] J. Keener and J. Sneyd. *Mathematical Physiology*. Springer-Verlag, New York, 2001.

[5] G. B. Ermentrout and D. Terman. *Mathematical Foundations of Neuroscience*. Springer, 2010.

[6] A. T. Winfree. *The geometry of biological time, 2nd ed.* Springer-Verlag, New York, 2001.

[7] I. R. Epstein and J. A. Pojman. *An introduction to nonlinear chemical dynamics*. Oxford University Press, 1998.

[8] R. J. Field and M. Burger. *Oscillations and traveling waves in chemical systems*. John Wiley & sons, 1985.

[9] I. R. Epstein and K. Showalter. Nonlinear chemical dynamics: Oscillations, patterns and chaos. *J. Phys. Chem.*, 100:13132–13147, 1996.

[10] V. K. Vanag, L. Yang, M. Dolnik, A. M. Zhabotinsky, and I. R. Epstein. Oscillatory cluster patterns in a homogeneous chemical system with global feedback. *Nature*, 406:(6794):389–391, 2000.

[11] V. K. Vanag, A. M. Zhabotinsky, and I. R. Epstein. Pattern formation in the Belusov-Zhabotinsky reaction with photochemical global feedback. *J. Phys. Chem. A*, 104:11566–11577, 2000.

[12] L. Yang, M. Dolnik, A. M. Zhabotinsky, and I. R. Epstein. Oscillatory clusters in a model of the photosensitive Belusov-Zhabotinsky reaction system with global feedback. *Phys. Rev. E*, 62(5):6414–6420, 2000.

[13] H. G. Rotstein, N. Kopell, A. Zhabotinsky, and I. R. Epstein. A canard mechanism for localization in systems of globally coupled oscillators. *SIAM J. Appl. Math.*, 63:1998–2019, 2003.

[14] H. G. Rotstein, N. Kopell, A. Zhabotinsky, and I. R. Epstein. Canard phenomenon and localization of oscillations in the Belousov-Zhabotinsky reaction with global feedback. *J. Chem. Phys*, 119 (17):8824–8832, 2003.

[15] A. F. Taylor, P. Kapetanopoulos, B. J. Whitaker, R. Toth, L. Bull, and M. R. Tinsley. Phase clustering in globally coupled photochemical oscillators. *Eur. Phys. J. Special Topics*, 165:137–149, 2008.

[16] D. Gonze, S. Bernard, C. Waltermann, A. Kramer, and H. Herzel. Spontaneous synchronization of coupled circadian oscillators. *Biophys. J.*, 89:107–119, 2005.

[17] D. Gonze, N. Markadieu, and A. Goldbeter. Selection of in-phase or out-of-phase synchronization in a model based on global coupling of cells undergoing metabolic oscillations. *Chaos*, 18:037127, 2008.

[18] M. Bertram, C. Beta, M. Pollmann, A. S. Mikhailov, H. H. Rotermund, and G. Ertl. Pattern formation on the edge of chaos: Experiments with CO oxidation on a Pt(110) surface under global delayed feedback. *Phys. Rev. E*, 67:036208, 2003.

[19] M. Bertram and A. S. Mikhailov. Pattern formation on the edge of chaos: Mathematical modeling of CO oxidation on a Pt(110) surface under global delayed feedback. *Phys. Rev. E*, 67:036207, 2003.

[20] Kim M., M. Bertram, M. Pollmann, A. von Oertzen, A. S. Mikhailov, H. H. Rotermund, and G. Ertl. Controlling chemical turbulence by global delayed feedback: Pattern formation in catalytic CO oxidation on Pt(110). *Science*, 292:1357–1360, 2001.

[21] F. Plenge, P. Rodin, E. Schöll, and K. Krischer. Breathing current domains in globally coupled electrochemical systems: A comparison with a semiconductor model. *Phys. Rev. E*, 64:056229, 2001.

[22] F. Plenge, Y.-J. Li, and K. Krischer. Spatial bifurcations in the generic N-NDR electrochemical oscillator with negative global coupling: Theory and surface plasmon experiments. *J. Phys. Chem. B*, 108:14255–14264, 2004.

[23] N. Baba and K. Krischer. Mixed-mode oscillations and cluster patterns in an electrochemical relaxation oscillator under galvanostatic control. *Chaos*, 18:015103, 2008.

[24] W. Wang, I. Z. Kiss, and J. L. Hudson. Experiments on arrays of globally coupled chaotic electrochemical oscillators: Synchronization and clustering. *Chaos*, 10:248–256, 2000.

[25] I. Z. Kiss, W. Wang, and J. L. Hudson. Populations of coupled electrochemical oscillators. *Chaos*, 12:252–263, 2002.

[26] I. Kiss, Y. Zhai, and J. L. Hudson. Resonance clustering in globally coupled electrochemical oscillators with external forcing. *Phys. Rev. Lett.*, 77:046204, 2008.

[27] V. García-Morales, A. Orlov, and K. Krischer. Subharmonic phase clusters in the complex Ginzburg-Landau equation with nonlinear global coupling. *Phys. Rev. E*, 82:065202, 2010.

[28] V. García Morales and K. Krischer. Normal-form apprach to spatiotemporal pattern formation in globally coupled electrochemical systems. *Phys. Rev. E*, 78:057201, 2008.

[29] M. A. Liauw, P. J. Plath, and N. I. Jaeger. Complex oscillations and global coupling during the catalytic oxidation of CO. *J. Chem. Phys*, 104:6375–6386, 1996.

[30] D. Golomb and J. Rinzel. Clustering in globally coupled inhibitory neurons. *Physica D*, 72:259–282, 1994.

[31] D. Terman and Wang D. L. Global competition and local cooperation in a network of neural oscillators. *Physica D*, 81:148–176, 1995.

[32] J. Rubin and D. Terman. Analysis of clustered firing patterns in synaptically coupled networks of oscillators. *J. Math. Biol.*, 41:513–545, 2000.

[33] D. M. Durand, E.-H. Park, and A. L. Jensen. Potassium diffusive coupling in neural networks. *Philos. Trans. R. Soc. B*, 365:2347–2362, 2010.

[34] M. G. Rosenblum and A. S. Pikovsky. Controlling synchronization in an ensemble of globally coupled oscillators. *Phys. Rev. Lett.*, 92:114102, 2004.

[35] R. A. Stefanescu and V. K. Jirsa. A low dimensional description of globally coupled heterogeneous neural networks of excitatory and inhibitory neurons. *PLoS Computational Biology*, 4:e1000219, 2008.

[36] K. Miyakawa and K. Yamada. Synchronization and clustering in globally coupled salt-water oscillators. *Physica D*, 151:217–227, 2001.

[37] S. Yu. Kourtchatov, V. V. Likhanskii, A. P. Napartovich, F. T. Arecchi, and A. Lapucci. Theory of phase locking of globally coupled laser arrays. *Phys. Rev. A*, 52:4089–4094, 1995.

[38] E. Alvarez-Lacalle, J. F. Rodriguez, and B. Echebarria. Oscillatory regime in excitatory media with global coupling: application to cardiac dynamics. *Computers in Cardiology*, 35:189–192, 2008.

[39] E. Alvarez-Lacalle and B. Echebarria. Global coupling in excitable media provides a simplified description of mechanoelectrical feedback in cardiac tissue. *Phys. Rev. E*, 79:031921, 2009.

[40] Y. Kuramoto. *Chemical Oscillations, Waves, and Turbulence*. Sringer-Verlag, Berlin, 1984.

[41] D. Golomb, D. Hansel, B. Shraiman, and H. Sompolinksy. Clustering in globally coupled phase oscillators. *Phys. Rev. A*, 45:3516–3530, 1992.

[42] D. Hansel, G. Mato, and C. Meunier. Clustering and slow switching in globally coupled phase oscillators. *Phys. Rev. E*, 48:3470–3477, 1993.

[43] P. Ashwin, G. Orozs, J. Wordsworth, and S. Townley. Dynamics on networks of cluster states for globally coupled phase oscillators. *SIAM J. Appl. Dyn. Syst.*, 6:728–758, 2007.

[44] E. Brown, P. Holmes, and J. Moehlis. Globally coupled oscillator networks. *In Perspectives and Problems in Nonlinear Science: A Celebratory Volume in Honor of Larry Sirovich, K. Sreenivasan, E. Kaplan, and J. Marsden, eds., Springer, New York*, pages 183–215, 2003.

[45] K. Y. Tsang, R. E. Mirollo, S. H. Strogatz, and K. Wiesenfeld. Dynamics of globally coupled oscillator arrays. *Physica D*, 48:102–112, 1991.

[46] S. H. Strogatz. From kuramoto to crawford: exploring the onset of synchronization in populations of coupled oscillators. *Physica D*, 143:1–20, 2000.

[47] A. M. Zhabotinksy. Periodic processes of malonic acid oxidation in a liquid phase. *Biofizika*, 9:306–311, 1964.

[48] A. M. Zhabotinksy. Belousov-Zhabotinsky reaction. *Scholarpedia*, 2:1435, 2007.

[49] B. P. Belousov. A periodic reaction and its mechanism. *Compilation of Abstracts on Radiation Medicine (Med. Publ., Moscow)*, 147:145, 1959.

[50] B. P. Belousov. A periodic reaction and its mechanism. *in Field, R. J. and Burger, M., Eds., Oscillations and traveling waves in chemical systems (Wiley, New York)*, 1985.

[51] A. M. Zhabotinsky, F. Buchholtz, A. B. Kiyatkin, and I. R. Epstein. Oscillations and waves in metal-ion-catalyzed bromate oscillating reactions in highly oxidized states. *J. Phys. Chem.*, 97:7578–7584, 1993.

[52] R. FitzHugh. Impulses and physiological states in models of nerve membrane. *Biophysical J.*, 1:445–466, 1961.

[53] R. FitzHugh. Mathematical models for excitation and propagation in nerve. *In: Biological Engineering. Schwan, H. P., editor (McGraw Hill: New York, New York)*, pages 1–85, 1969.

[54] J. S. Nagumo, S. Arimoto, and S. Yoshizawa. An active pulse transmission line simulating nerve axon. *Proc. IRE*, 50:2061–2070, 1962.

[55] H. Morris, C.a nd Lecar. Voltage oscillations in the barnacle giant muscle fiber. *Biophysical J.*, 35:193–213, 1981.

[56] X.-J. Wang and J. Rinzel. Alternating and synchronous rhythms in reciprocally inhibitory model neurons. *Neural Computation*, 4:84–97, 1992.

[57] F. K. Skinner, N. Kopell, and E. Marder. Mechanisms for oscillations and frequency control in networks of mutually inhibitory relaxation oscillators. *Journal of Computational Neuroscience*, 69-87, 1994.

[58] N. Kopell and G. B. Ermentrout. Mechanisms of phase-locking and frequency control in pairs of coupled neural oscillators. *In Handbook on Dynamical Systems: Toward applications. Ed. B. Fiedler, Elsevier*, 2:3–54, 2002.

[59] A. Birzu and K. Krischer. Resonance tongues in a system of globally coupled oscillators with time-periodic coupling strength. *Chaos*, 20:043114, 2010.

[60] M. Somani, M. A. Liwuw, and D. Luss. Evolution and impact of temperature patterns during hydrogen oxidation on a Ni ring. *Chem. Engg. Sci.*, 52:2331, 1997.

[61] C. G. Assisi, V. K. Jirsa, and J. A. Kelso. Synchrony and clustering in heterogeneous networks with global coupling and parameter dispersion. *Phys. Rev. Lett.*, 94:018106, 2005.

[62] X. R. Sailer, V. Beato, L. Schimansky-Geier, and H. Engel. Noise-induced effects in excitable systems with local and global coupling. *In Analysis and control of complex nonlinear processes in physics, chemistry and biology. L. Schimansky-Geier, B. Fiedler, J. Kurths, E. Scholl, eds. (World Scientific)*, pages 1–42, 2007.

[63] D. Golomb, X.-J. Wang, and J. Rinzel. Synchronization properties of spindle oscillations in a thalamic reticular nucleus model. *J. Neurophysiol.*, 72:1109–1126, 1994.

[64] J. Rubin and D. Terman. Geometric analysis of population rhythms in synaptically coupled neuronal networks. *Neural Computation*, 12:597–645, 2000.

[65] Wang D. L. and D. Terman. Locally excitatory globally inhibitory oscillator networks. *IEEE Transactions on Neural Networks*, 6 (1):283–286, 1995.

[66] F. Dumortier and R. Roussarie. Canard cycles and center manifolds. *Memoirs of the American Mathematical Society*, 121 (577):1–100, 1996.

[67] W. Eckhaus. Relaxation oscillations including a standard chase on French ducks. *In Lecture Notes in Mathematics, Springer-Verlag*, 985:449–497, 1983.

[68] S. M. Baer and T. Erneux. Singular Hopf bifurcation to relaxation oscillations. *SIAM J. Appl. Math.*, 52:1651–1664, 1992.

[69] E. Benoit, J. L. Callot, F Diener, and Diener M. *Chasse au Canard*, volume 31. Collect. Math., 1981.

[70] M. Krupa and P. Szmolyan. Relaxation oscillation and canard explosion. *J. Diff. Eq.*, 174:312–368, 2001.

[71] M. Krupa and P. Szmolyan. Extending geometric singular perturbation theory to nonhyperbolic points - fold and canard points in two dimensions. *SIAM J. Math. Anal.*, 33(2):286–314, 2001.

[72] F. Dumortier. Techniques in the theory of local bifurcations: Blow-up, normal forms, nilpotent bifurcations, singular perturbations. *In Bifurcations and Periodic Orbits of Vector Fields, edited by D. Schlomiuk (Kluwer Academic Press, Dordrecht)*, pages 19–73, 1993.

[73] J. Guckenheimer and P. Holmes. *Nonlinear oscillations, dynamical systems, and bifurcations of vector fields*. Springer-Verlag, New York, 1983.

[74] H. G. Rotstein, S. Coombes, and A. M. Gheorghe. Canard-like explosion of limit cycles in two-dimensional piecewise-linear models of FitzHugh-Nagumo type. *SIAM J. Appl. Dyn. Systems*, 11:135–180, 2012.

[75] H. G. Rotstein, S. Coombes, and A. M. Gheorghe. Canard-like explosion of limit cycles in two-dimensional piecewise-linear models of FitzHugh-Nagumo type. *NJIT CAMS Technical Report*, 1112-4:1–60, 2011.

[76] M. Wechselberger. Existence and bifurcation of canards in R^3 in the case of a folded node. *SIAM J. Appl. Dyn. Syst.*, 4:101–139, 2005.

[77] M. Brøns, M. Krupa, and M. Wechselberger. Mixed mode oscillations due to the generalized canard phenomenon. *in Fields Institute Communications Bifurcation theory and spatio-temporal pattern formation, Wayne Nagata, N. Sri Namachchivaya (Eds.)*, 49:39–63, 2006.

[78] M. Desroches, J. Guckenheimer, B. Krauskopf, C. Kuehn, H. M. Osinga, and M. Wechselberger. Mixed-mode oscillations with multiple time scales. *To be published in SIAM Reviews*, 2012.

[79] D. Terman, N. Kopell, and A. Bose. Dynamics of two mutually coupled slow inhibitory neurons. *Physica D*, 117:241–275, 1998.

[80] N. Kopell and D. Somers. Anti-phase solutions in relaxation oscillators coupled through excitatory interactions. *J. Math. Biol.*, 33:261–280, 1995.

[81] D. Somers and N. Kopell. Rapid synchrony through fast threshold modulation. *Biol. Cybern.*, 68:393–407, 1993.

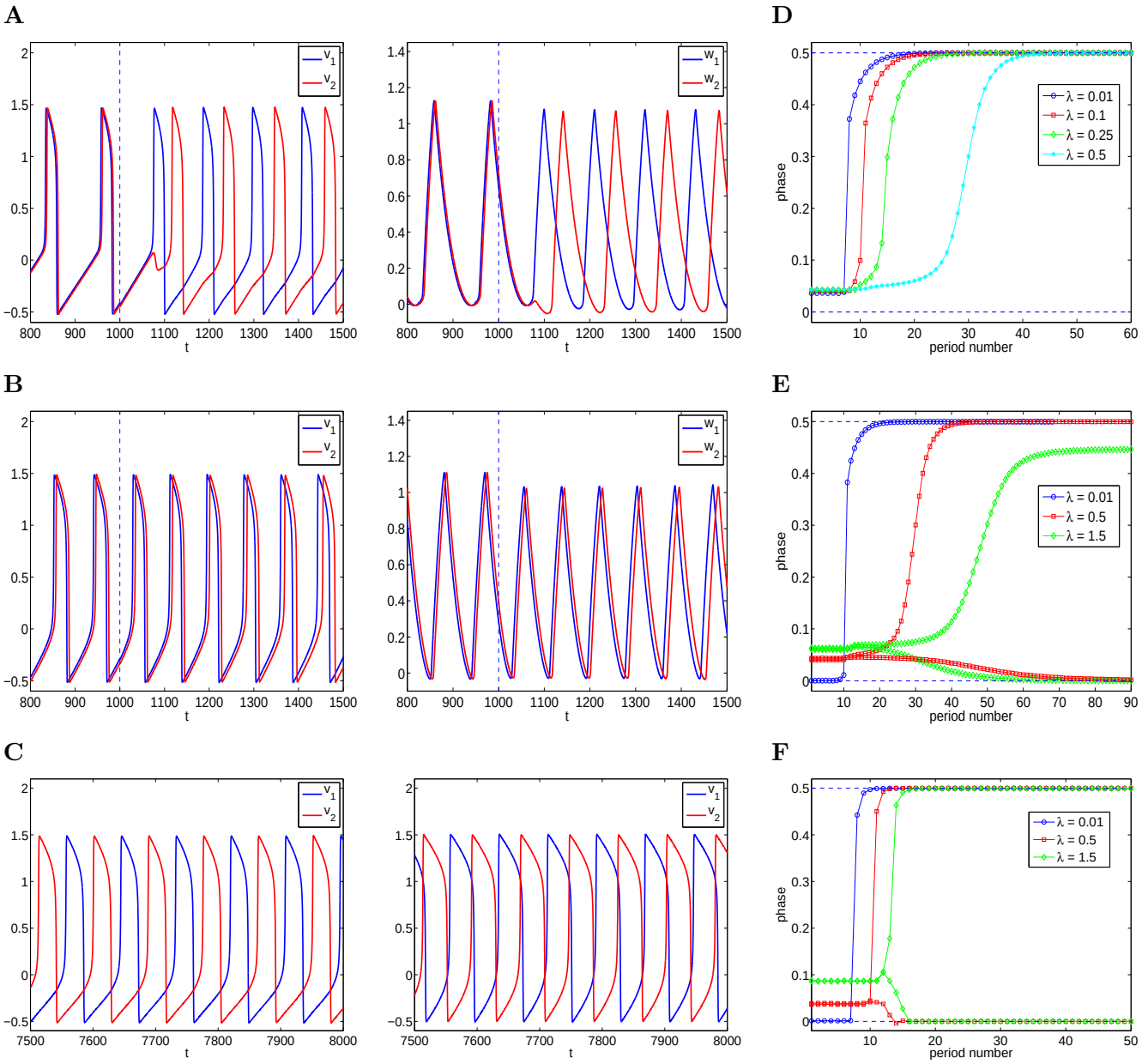

Figure 8: **Oscillatory patterns for the globally coupled FHN model. A to C:** v- and w-traces for various values of λ. In all panels, global coupling was "activated" at $t = 1000$, and the two oscillators were decoupled before that. The vertical dashed-lines indicates this time. **A:** $\lambda = 0.01$. **B:** $\lambda = 0.5$. **C:** $\lambda = 0.5$ (left) and $\lambda = 1.5$ (right). **D to F:** Graphs of phase as a function of the period number for various values of λ. **D and E:** $\gamma = 0.1$. **F:** $\gamma = 2$. Panel D illustrates the dependence of the "pace" of cluster formation on the parameter λ. Panels E and F illustrates the basin of attraction of of phase-locked and in-phase patterns for various values of λ. We used the following parameter values: $\alpha = 4$, $\epsilon = 0.01$, $\sigma_1 = 0.5 = \sigma_2 = 0.5$, and $\gamma = 0.1$ (except in panel F).

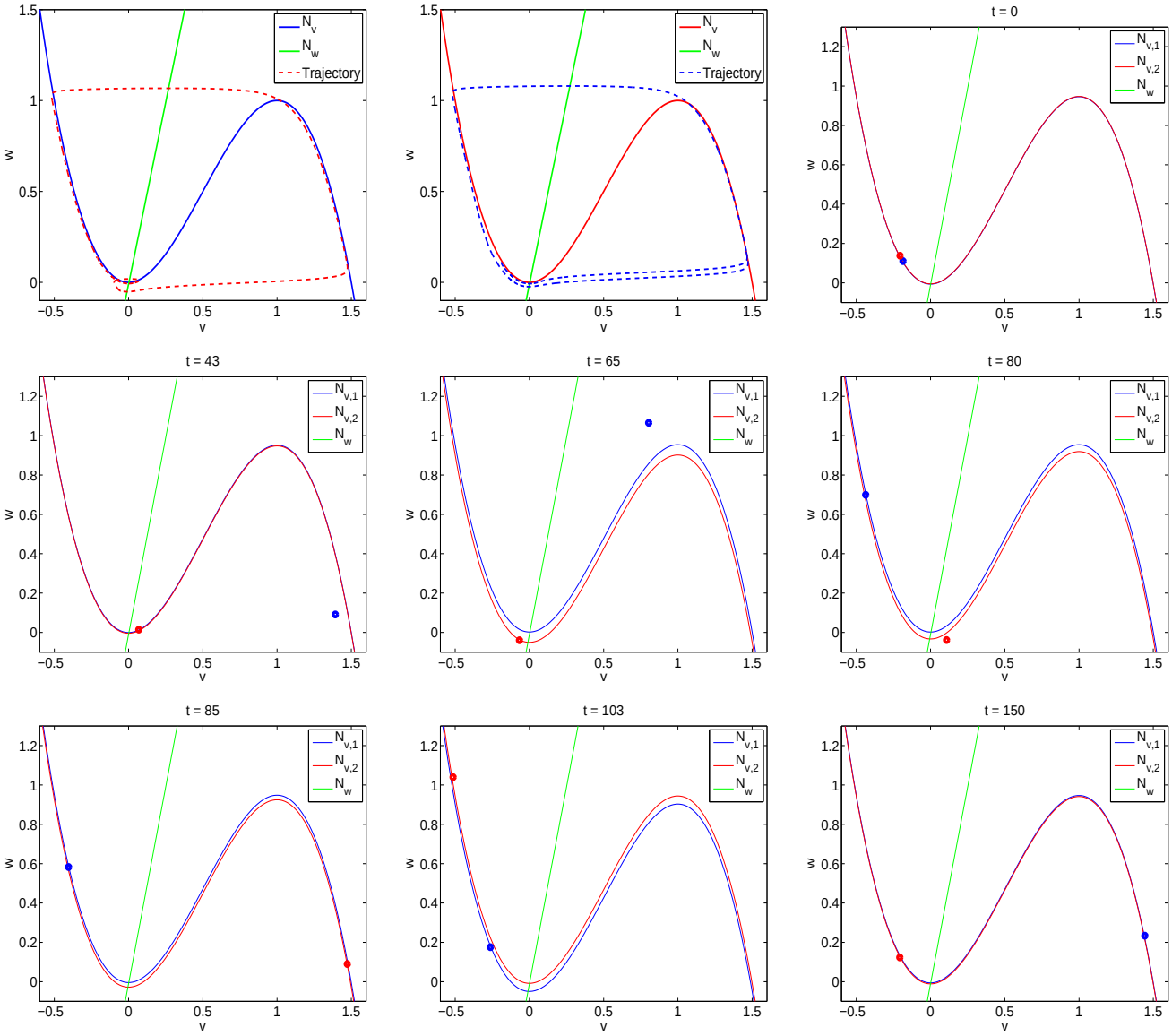

Figure 9: **Generation of antiphase patterns in the globally coupled FHN model. The v- and w-traces are shown in Fig. 8-A. The first two panels show the full trajectories for the two oscillators.** We used the following parameter values: $\alpha = 4$, $\epsilon = 0.01$, $\lambda = 0.01$, $\gamma = 0.1$, $\sigma_1 = \sigma_2 = 0.5$.

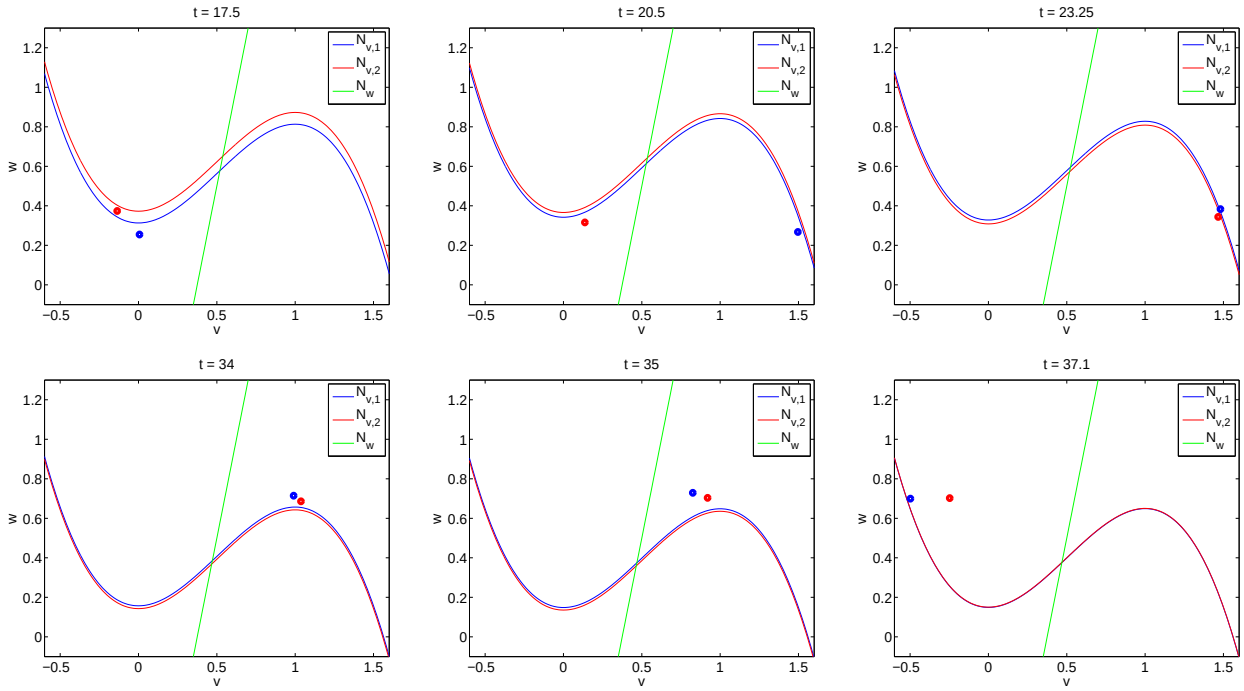

Figure 10: **In-phase synchronization in the globally coupled FHN model.** We used the following parameter values: $\alpha = 4$, $\epsilon = 0.01$, $\lambda = 1.5$, $\gamma = 2$, $\sigma_1 = \sigma_2 = 0.5$.

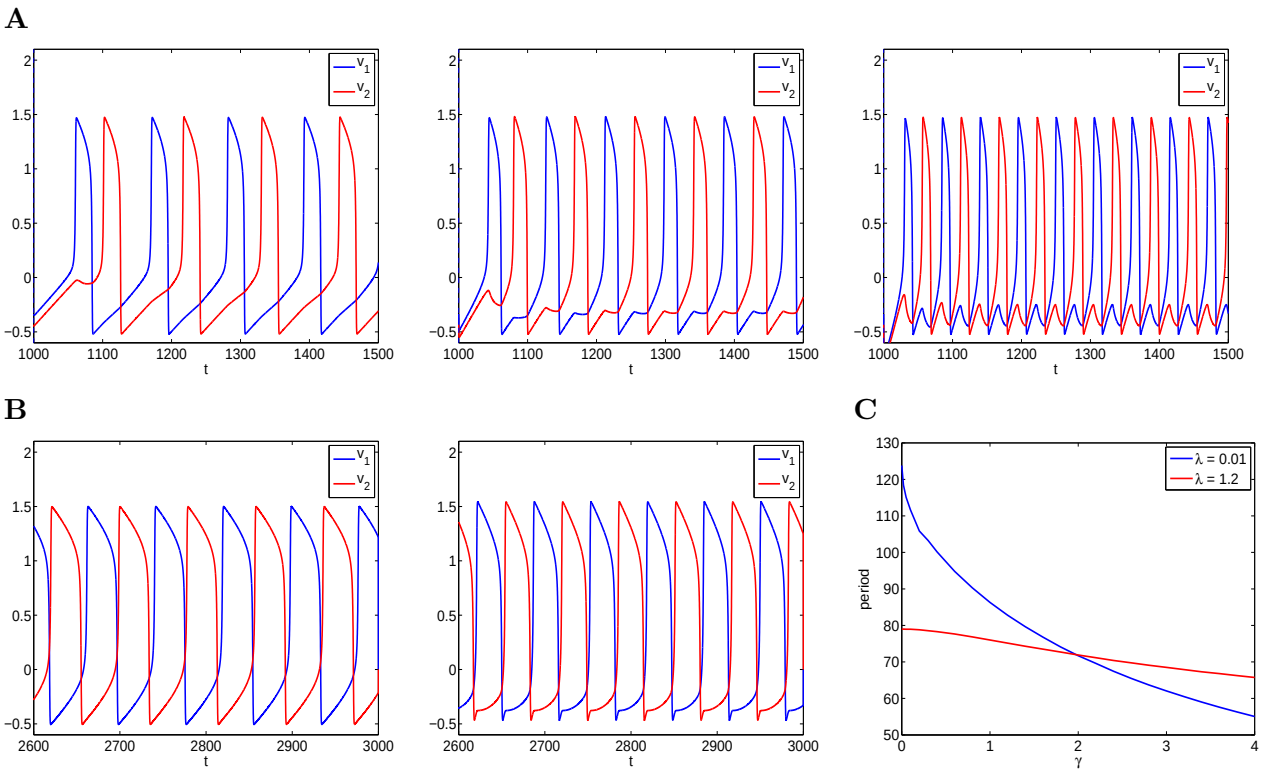

Figure 11: **Oscillatory patterns for the globally coupled FHN model. The oscillatory frequency increases with the global coupling parameter. A:** v-traces for $\lambda = 0.01$, and $\gamma = 0.1$ (left), $\gamma = 1$ (middle) and $\gamma = 4$ (right). **B:** v-traces for $\lambda = 1.2$, and $\gamma = 0.1$ (left) and $\gamma = 4$ (right). **C:** Oscillatory period as a function of γ for $\lambda = 0.01$ and $\lambda = 1.2$. We used the following parameter values: $\alpha = 4$, $\epsilon = 0.01$, $\sigma_1 = \sigma_2 = 0.5$.

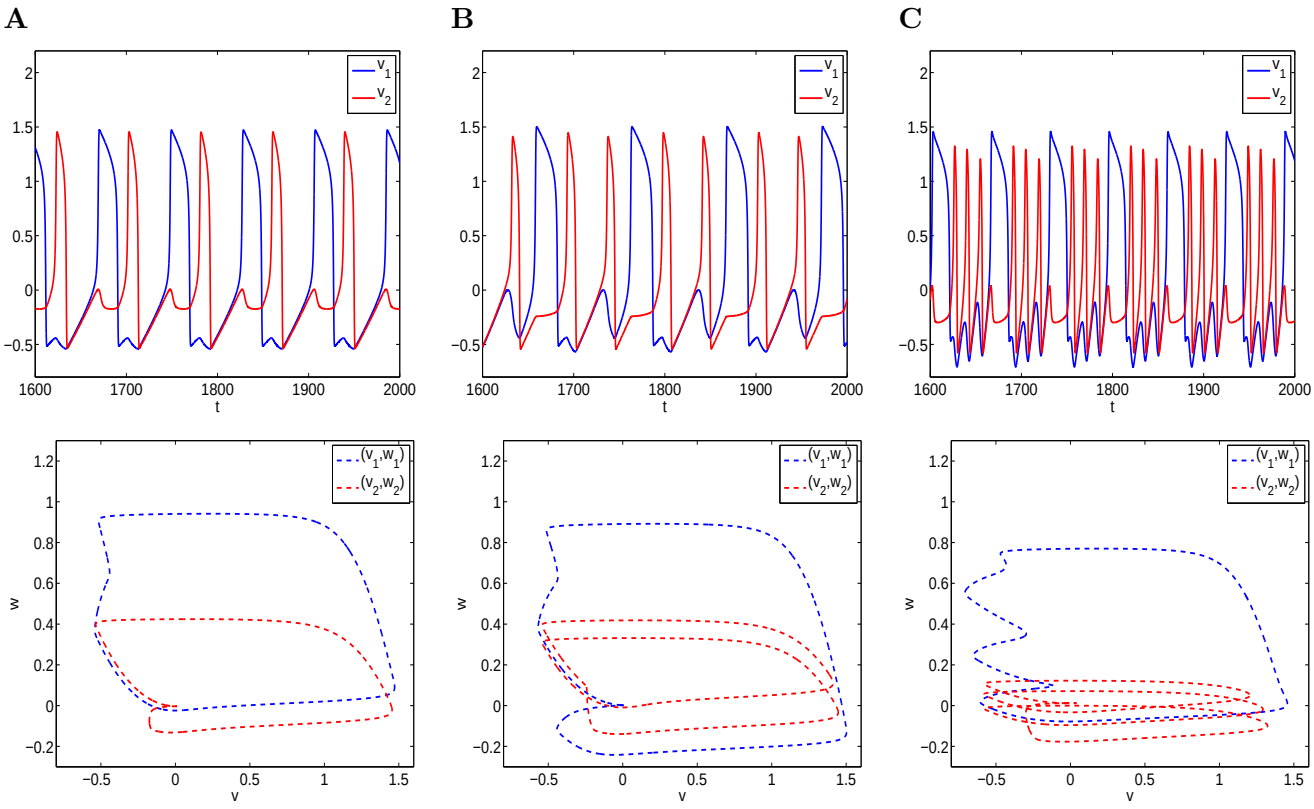

Figure 12: **Oscillatory patterns for the globally coupled FHN model for** $\sigma_1 = 0.2$, $\sigma_2 = 0.8$, $\lambda = 0.01$, $\epsilon = 0.01$, $\alpha = 4$ **and various representative values of** γ**.** Top panels show the v-traces and bottom panels show the corresponding trajectories. **A:** $\gamma = 2$. **B:** $\gamma = 2.8$. **C:** $\gamma = 15$.

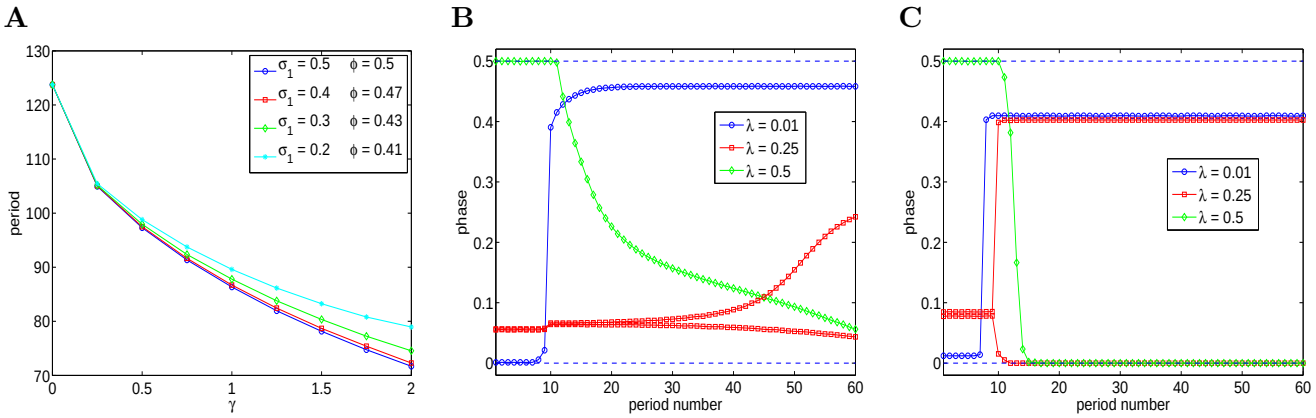

Figure 13: **Oscillatory patterns for the globally coupled FHN model. A.** The oscillatory frequency increases with the global coupling parameter for all cluster sizes (σ_1) and decreases with increasing values of the cluster size difference. We used the following parameter values: $\alpha = 4$, $\epsilon = 0.01$, $\lambda = 0.01$, $\gamma = 1$. **B.** Graphs of phase as a function of the period number for various values of λ for $\gamma = 0.1$. **C.** Graphs of phase as a function of the period number for various values of λ for $\gamma = 1$. In B and C we used the following parameter values: $\alpha = 4$, $\epsilon = 0.01$, $\sigma_1 = 0.2$, $\sigma_2 = 0.8$.

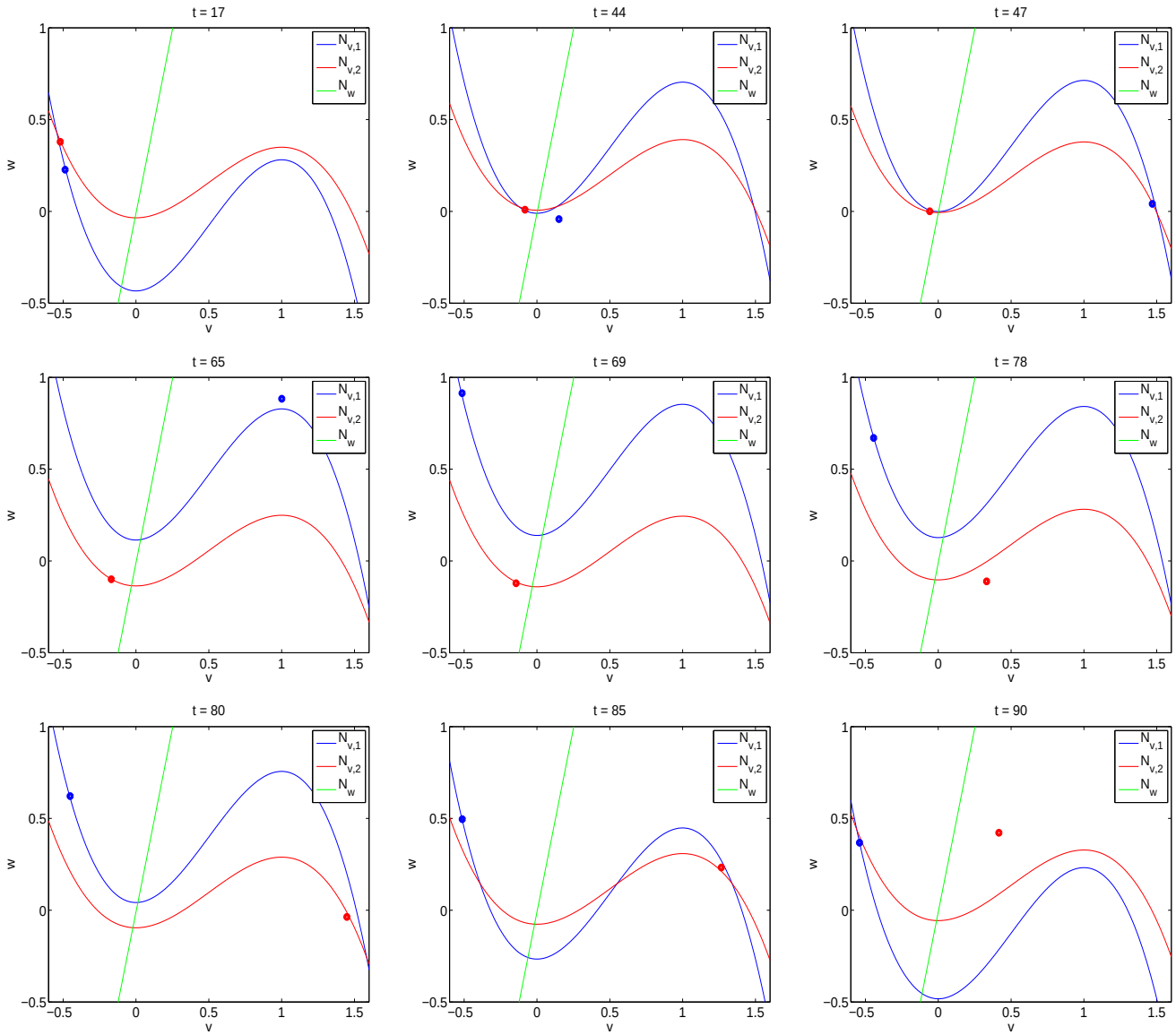

Figure 14: **Generation of 1:1 phase-locked patterns in the globally coupled FHN model with different cluster sizes.** We used the following parameter values: $\alpha = 4$, $\epsilon = 0.01$, $\lambda = 0.01$, $\gamma = 2$, $\sigma_1 = 0.2$, $\sigma_2 = 0.8$. Fig. 12-A.

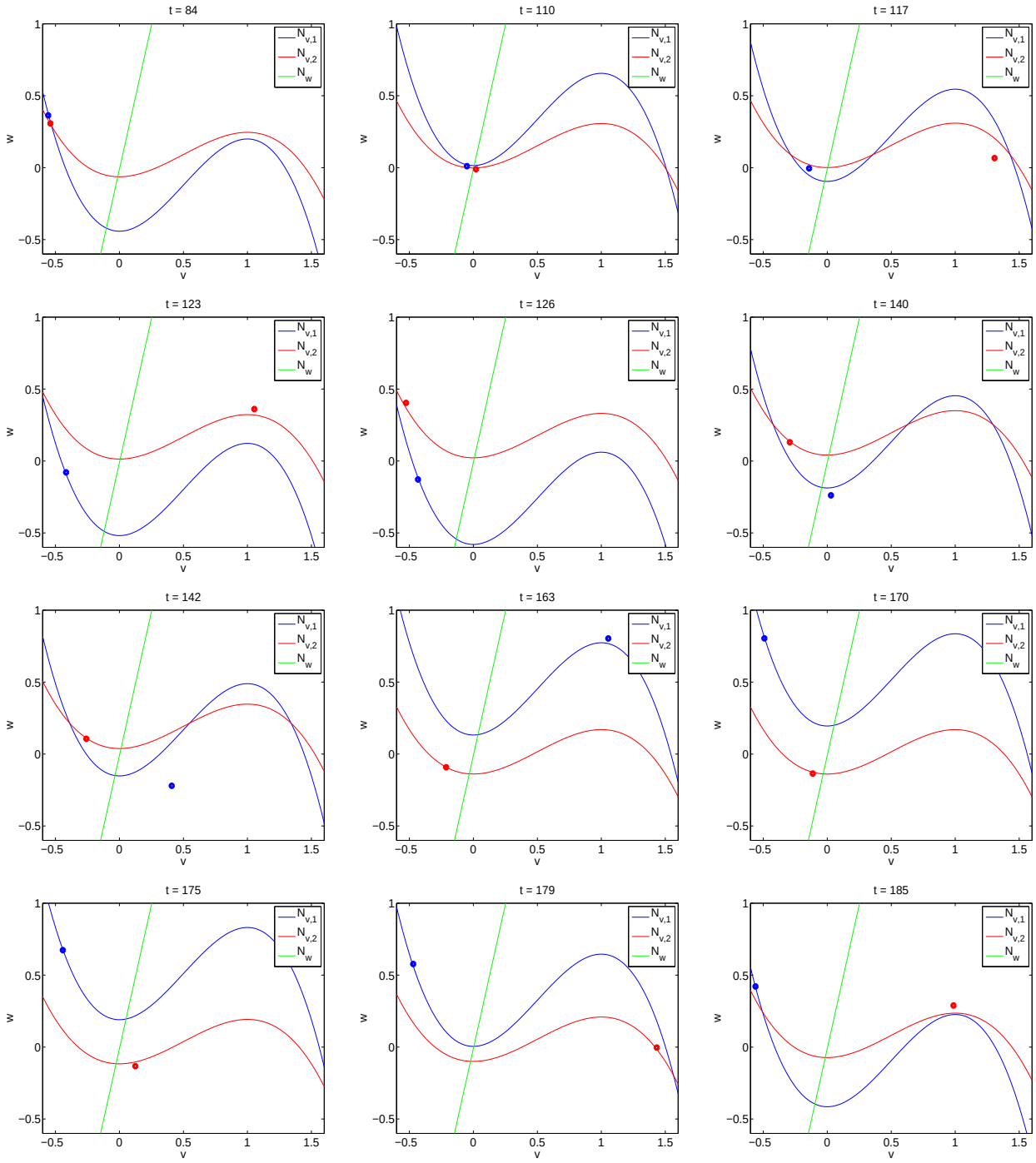

Figure 15: **Generation of 2:1 phase-locked patterns in the globally coupled FHN model with heterogeneous cluster sizes.** We used the following parameter values: $\alpha = 4$, $\epsilon = 0.01$, $\lambda = 0.01$, $\gamma = 2.8$, $\sigma_1 = 0.2$, $\sigma_2 = 0.8$. Fig. 12-B.